Energy, exergy, and economic analyses of a novel biomass-based multigeneration system integrated with multi-effect distillation, electrodialysis, and LNG tank

Yan Cao, M. Kasaeian, H. Abbasspoor, Moein Shamoushaki, M.A. A Ehyaei, Stéphane Abanades

Energy, exergy, and economic analyses of a novel biomass-based multigeneration system integrated with multi-effect distillation, electrodialysis, and LNG tank

Yan Cao[1], M Kasaeian[2], H. Abbasspoor[3], Moein Shamoushaki[4], M. A. Ehyaei[5*], Stéphane Abanades[6]

[1] School of Mechatronic Engineering, Xi'an Technological University, Xi'an, 710021 China

[2]Department of Environmental Economics, Science and Research Branch, Islamic Azad University, Tehran, Iran

[3]Department of Biology, Faculty of Biological Science, North Tehran Branch, Islamic Azad University, Tehran, Iran

[4] Department of Industrial Engineering, University of Florence, Florence, Italy

[5] Department of Mechanical Engineering, Pardis Branch, Islamic Azad University, Pardis City, Iran

[6] Processes, Materials, and Solar Energy Laboratory, PROMES-CNRS, 7 Rue du Four Solaire, 66120 Font-Romeu, France

*Corresponding author: aliehyaei@yahoo.com

Abstract

In this study, a novel multigeneration system is considered from energy, exergy, and economic points of view. The combined system composed of biomass gasifier, CO_2 cycle, cooling system, multi-effect distillation (MED), and electrodialysis was assessed. This integrated system produces electricity, cooling, distilled water, sodium hydroxide (NaOH), and hydrogen chloride (HCl). A parametric study regarding moisture content of biomass, the efficiency of expander I, LHV of biomass, the salt concentration of seawater, and a number of MED effects on system performance was conducted. The obtained energy and exergy efficiencies of modeled MGS are 75.1% and 88.4%. The highest and lowest exergy destruction rates (EDR) belong to the liquefied natural gas line and electrodialysis, respectively. The proposed MGS produces 73.17 GWh of cooling, 103 GWh of electrical energy, 1223 Ton of NaOH, 1114 Ton of HCl, and 212.6 m^3 of potable water annually. The influence of expander I on energy and exergy efficiencies of the CO_2 cycle was investigated. Results revealed that increasing the LHV of the biomass results in a decrement of both energy and exergy efficiencies of MGS and recovery ratio. When considering the biomass moisture content, the efficiencies of exergy and exergy of MGS diminished with a rise in moisture amount.

Keywords: Multi-generation system; Multi-effect distillation; Electrodialysis; Exergy; Economic

1) Introduction

One of the most severe challenges threatening human society is global warming. Based on recent studies, greenhouse gas (GHG) release is expected to rise by 50% and become the most dominant adverse factor responsible for climate change by 2050 [1]. The GHG principally originates from fossil fuels combustion. Therefore, the substitution of fossil fuels with clean energies is vital. The application of biomass-originated energy systems has been identified as a promising solution [2, 3]. Biomass gasification is an economic and high-efficiency method that makes possible biomass transformation to clean and flammable gaseous stocks using a gasifier [4]. The method's effectiveness remarkably influences the provided syngas yield and quality [5].

Besides, deficiency of water is a significant vital global concern endangering nowadays [6]. The United Nations reported that in 2050, nearly seven billion people in sixty nations would face drastic scarcity of water [7]. Seawater desalination is noticed as a viable and most used technique to cope with the growing requirement for cleaner water [8]. There are two main kinds of seawater desalination processes to produce distilled water (DW). The first is named the thermal desalination system (TES). Seawater is transformed to vapor by evaporation process and then chilled into purified water. Another approach comprises desalination methods promoted through diverse separation techniques like reverse osmosis (RO) [9]. Two attractive approaches in thermal desalination are the multi-effect evaporation desalination (MED) and multi-stage-flash (MSF) evaporation desalination [10]. MED continues as an attractive choice due to the lower rate of corrosion, the power needed, and the costs of desalted water compared with MSF [11].

Desalination of seawater provides a rich source of fresh water, a crucial supply for people's well-being and farming. While the application of desalination proceeds to expand, high-salinity brine evacuation is an environmental matter, causes a possible adverse consequence on the ecosystems [12]. The global brine production is about 141.5 million m^3/day, which is principally released into ocean habitats [13]. As desalination application continues to develop, discharge of high-salinity brine could harm the environment and ecosystems. To improve the economic and environmental aspects of the desalination of seawater, developing technology to generate HCl and NaOH with low power use is essential. Chemical products on-site production from brine could eliminate the need of purchasing and transporting chemicals from elsewhere. The negative consequences of discharge of the brine on the environment and ecosystem

could be minimized by recovering the chemical resources of the brine. In addition, it makes it possible to recycle back brine to the freshwater partially [14].

Junjie et al. [15] proposed a cogeneration power cycle integrated with an improved MSF desalination mechanism. They showed that the concentration of the brine in each stage and the average yearly capital expense of freshwater generation is possible to decline by 21.8% and 10.7%, respectively, compared with conventional MSF. Meratizaman et al. [16] studied a unified system composed of MED, solid oxide fuel cell (SOFC), and gas turbine (GT) cycles. For the economic assessment, the yearly expense is applied. Their conclusions revealed that the integration of MED and SOFC-GT systems improved the cycle economically. Najafi et al. [17] analyzed a SOFC-GT-MSF linked system exegetically, economically, and environmentally. They optimized this cycle by a multi-objective genetic algorithm (MOGA) to obtain the optimum operating variables. Their achieved outcomes confirmed that exergetic productivity and whole expense were achieved at optimum point, namely 46.7% and 3.76 million USD/year, respectively. Mokhtari et al. [18] evaluated a combined cycle including GT, MED, and RO systems to produce water and electricity in the Iran southern region in the outskirts of the Persian Gulf. According to their analysis, higher than required energy led to a decrease of 0.5 dollars per m^3 in unit product cost while a hybrid cycle is implemented. Shamoushaki et al. [19] conducted thermodynamic, exergy, economic and environmental evaluation of hybrid cycle composed of SOFC-GT systems. The multi-objective optimization of the integrated system by non-dominated sorting genetic algorithm II (NSGA-II) was conducted. They calculated the cost rate, 0.0435 US$/s, and efficiency of exergy of 57.7% at the optimum point. Also, the payback time was obtained at about 3.12 years.

Khanmohammadi and Atashkari [20] proposed a new multigeneration biomass-based cycle combined with a desalination unit to provide electricity, fresh water, and hot water. The optimization has been carried out using the genetic algorithm to determine the optimum design variables amount. The combustion chamber and gasifier had the highest values of exergy destruction ratio (approximately 84%). Moghimi et al. [21] assessed a combined cooling, heating, and power (CCHP) hybrid cycle composed of GT, MED-thermal vapor compression (TVC), and ejector refrigeration cycle (ERC). The obtained exergy efficiency of the combined system was 2.1% greater than the single Brayton system. Also, their analyzed cycle showed a power production of 30 MW, cooling and heating capacities of 3.14 MW, and freshwater production of 85.57 kg/s. Rashidi and Khorshidi [22] studied a biomass gasification-based system for generating CCHP based on the exergy concept. The multi-objective optimization and fuzzy clustering methods were applied to find the optimum solution. They compared the obtained results with two diverse

optimization approaches, and the fruitfulness of the recommended process was validated employing different execution indicators. Ghaebi and Ahmadi [23] modeled a SOFC-GT system integrated with humidification-dehumidification (HDH) desalination and heat recovery steam generator (HRSG) units. The obtained results showed that the combined cycle produces heating, net electricity, and distilled water (370.2 kW, 1605 kW, and 345.7 kg/h, respectively). Mohammadi et al. [24] compared six different configurations of trigeneration systems based on the GT cycle. Diverse desalination and chiller systems were united with a coupled cycle. The consequences explicated the most reliable cost-effective arrangement was gas turbine combined cycle with wet cooling tower integrated with double effect absorption chiller (DEABC) and RO. Energetic and economic analysis of biomass-based integrated cycle with ORC to heat recovery and carbon storage has been performed by Georgousopoulos et al. [25]. 4.61% efficiency of combined system improvement has been achieved by proposing this system.

Vojdani et al. [26] performed the techno-economic and environmental assessment and multi-objective optimization of a cogeneration system composed of MED and SOFC-GT. According to the proposed system, the generated power, efficiency of exergy, and emission increased up to 6.5%, 8.4%, and 5.8% as opposed to SOFC-GT standalone system. Zoghi et al. [27] assessed a biomass-driven multi-production cycle composing a modified Kalina-LNG subsystem, electrolyzer, and thermoelectric generator. They calculated hydrogen and natural gas mass flow rates at 5.77 kg/h and 4.42 kg/s. Cao et al. [28] studied a new hybrid biomass-solar-based coupled system combined with hydrogen production. The multi-objective optimization of the system was carried out according to power cost and CO_2 emissions. The results showed that at the optimum solution, exergetic efficiency, Levelized cost of energy (LCOE), and carbon dioxide emission were 30.4%, 61.4 $/MWh, and 0.46 kg/kWh. Lak Kamari et al. [29] investigated an integrated system based on biofuel to generate electricity, bio-products, and heat. Their assessment showed 15% energy saving is possible with the designed system. Exergy, economic, exergonic, and optimization of a multipurpose cycle were done by Safder et al. [30]. The optimization outcomes determined that the combined system produced electricity, cooling, and freshwater (28.7 MW, 13.6 kg/s, and 3.4 MW, respectively). Thermo-economic evaluation of a biomass/natural gas-driven combined system has been studied by Jalili et al. [31]. The highest and lowest irreversibilities were related to gas cycle and double-effect absorption unit with 61% and 6% of total exergy destruction, respectively. Cao et al. [32] assessed a biomass gasification-fueled triple combined system from a thermos-economic aspect. The optimization of the integrated cycle was performed by a genetic algorithm to minimize the LCOE. The system showed a 6.7% higher efficiency applying CO_2 as a working fluid instead of helium. Xu et al. [33] studied a multi-production cycle including solid oxide electrolyzer, desalination, and ORC units supplied

by biomass energy. Exergy efficiency and cost are obtained at 17.16% and 26 $/GJ at optimized results. Musharavati et al. [34] conducted a combined system optimization to produce power and freshwater. Optimized electricity generation and desalinated water are obtained at 5127 kW and 38.6 kg/s.

Based on the above previous researches, there are no studies regarding a configuration of the multigeneration system (MGS) powered by biomass to produce electrical power, cooling, DW, sodium hydroxide (NaOH), and hydrogen chloride (HCl). In this MGS, steam is provided via biomass; then, this produced steam meets the energy needs of the CO_2 cycle and MED. In addition, liquid natural gas (LNG) is used as a heat sink to decrease the condenser pressure and increase the electrical power production via the CO_2 cycle. After absorbing heat from the condenser of the CO_2 cycle, the NG is used via an expansion turbine and cooler to produce electrical power and cooling. Also, another subsystem is added to MGS for the brine (B) discharge treatment. To be brief, the innovative aspects of the present study are as follows:

(i) Proposal of a novel configuration of MGS powered by biomass

(ii) Investigation of brine treatment to decrease the effects of B release on the environment.

(iii) Comprehensive system analyses include energy, exergy, and economic analyses

2) Methodology

2.1. Model configuration

Figure 1 depicts the system configuration. In the gasifier, biomass in the presence of heat is converted to biogas (points 1, 2, 3). The hot syngas heats the pressurized water via heater (points 3, 4, 5, 23). The syngas is burned in the boiler to convert hot water to steam (points 6 to 8). The steam is divided into two streams (points 9 & 10). The steam in point 9 is used in a multi-effect distillation (MED) system to produce demineralized water (DW) from the seawater (SW) (points 12 & 13). The part of dissipated brine (B) is converted to NaOH and HCl via electrodialysis (ELECD) (points 14 to 16). Another part of steam (point 10) meets the energy needs of the carbon dioxide (CO_2) cycle evaporator (Eva) (points 18, 20 to 21). In the CO_2 cycle, the liquefied CO_2 is used as a working fluid. This cycle operates similarly to the Rankine cycle. The liquefied CO_2 is pressurized via pump I (PI). Then, it transfers the heat with steam within the Eva to change to superheated steam (SHS) (points 10, 18, 20 to 21). The SHS rotates the expander I (EXP I) and generator (G) to produce electricity (points 21 & 22). The low-pressure steam flows through a condenser to dissipate heat and change to saturated liquid. Since the CO_2 cycle condenser temperature is lower than the environment, the liquefied natural gas (LNG) is used for this target (points 19, 22, 24 to 25). In the LNG line, the high-pressure LNG absorbs the heat from the CO_2 low-pressure steam (points 24 & 25). Then, it

157 expands through expander II (EXP II) and G to produce electricity. Furthermore, the low pressure and cold
158 LNG is used in the cooler to produce cooling (points 26 & 27). Figure 2 shows the layout of the MED. MED
159 works based on subsequent evaporation and condensation in different stages named effects. This system
160 converts the seawater (SW) to the demineralized (DW) and brine (B). Steam flows through tube bundles
161 (point 9), and it is used to evaporate the sprayed SW on the tube bundles. Then, it is condensed as DW.
162 The parts of SW sprayed on tube bundles evaporate and go to the second effect, and part of it accumulates
163 in the bottom of the effect and goes to the flash boxes, which contain more salt than seawater. This part
164 of B is evaporated in the flash boxes due to pressure drop arising from the effect to the flash box, and it
165 goes to the second effect. The non-evaporated B is dissipated to the environment. This process continues
166 until the last effect. The connection between subsystems and components is depicted in Figure 3.

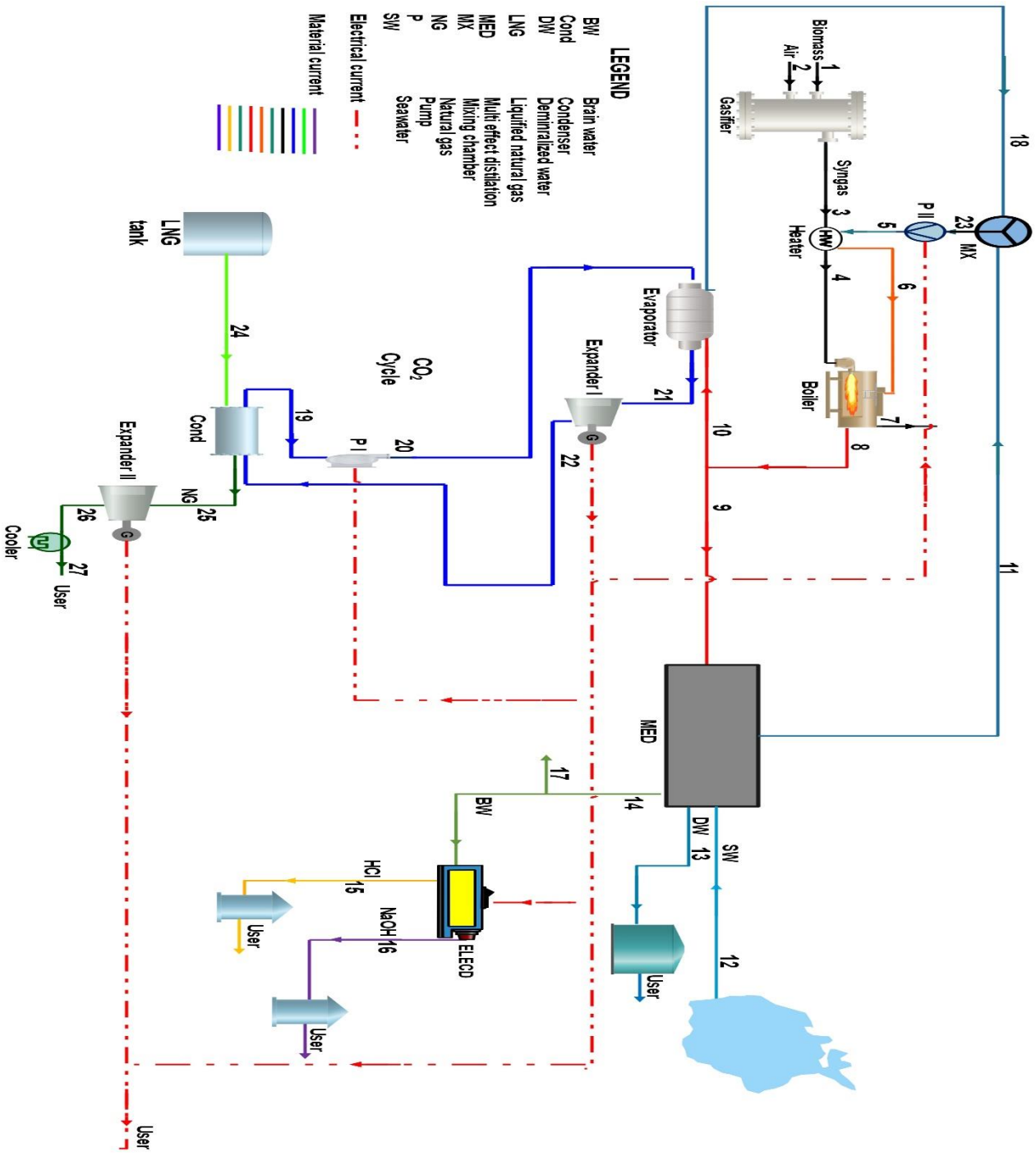

167

168 Figure 1. The layout of the proposed system

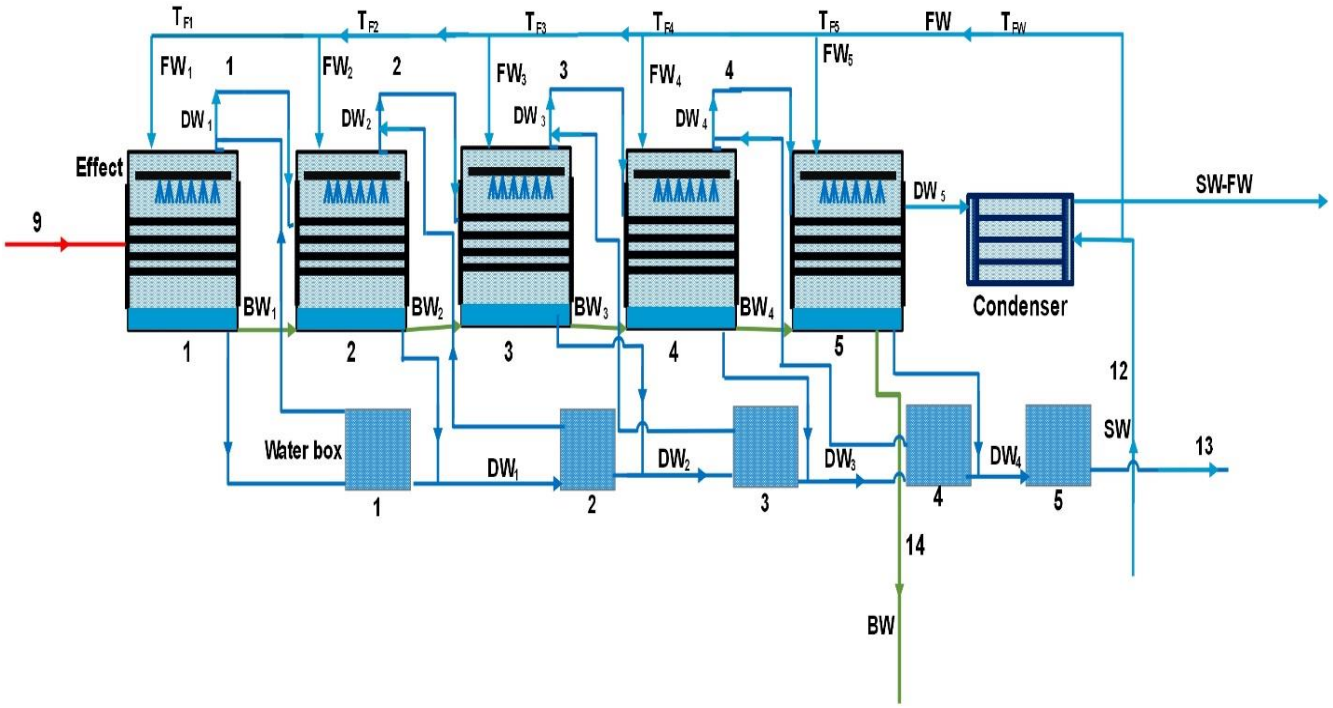

169

170 Figure 2. The layout of the MED

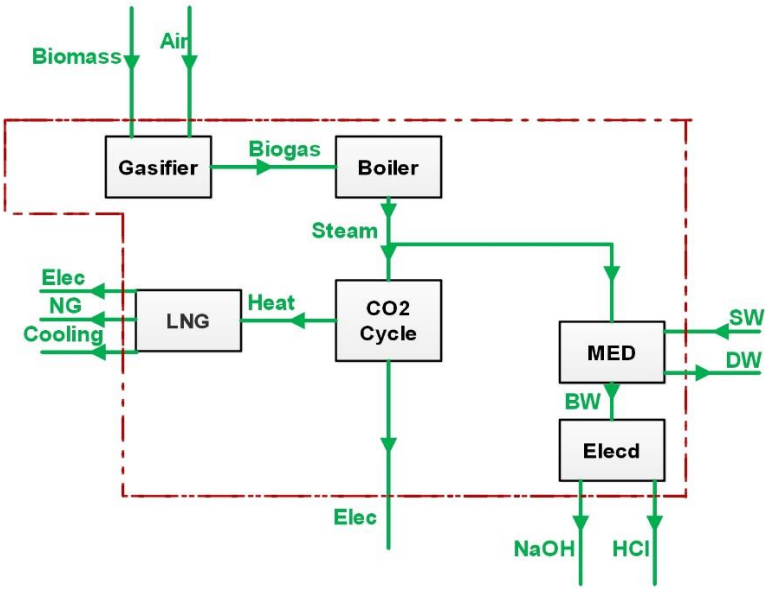

171

172 Figure 3. The connection/interaction between subsystems and components

173 **2.2. Energy and mass balance assessment**

174 The following assumptions are noticed for the energy assessment [35-39]:

175 1. The system operates at steady-state conditions.

2. The dead-state temperature and pressure are 15 ℃ and 101.3 kPa.
3. The heat losses are neglected.
4. The thermodynamic procedure in P and EXP is supposed polytropic, and the efficiency is assumed to be 85%.
5. Kinetic and potential energy are ignored.
6. DW and B have the effect temperature at the exit.
7. The overall heat transfer coefficient in MED is a function of temperature.
8. The temperature difference between each effect is equal.
9. The MED feed water is distributed equally.
10. The heat exchanger effectiveness factor is 85%.

The general mass and energy balance equations are shown below [40]:

$$\sum_{in} \dot{m} = \sum_{out} \dot{m} \tag{1}$$

$$\dot{Q} - \dot{W} + \sum_{in} \dot{m}\left(h + \frac{V^2}{2} + gZ\right) = \sum_{out} \dot{m}\left(h + \frac{V^2}{2} + gZ\right) \tag{2}$$

where $\dot{m}$, *h, V,* $\dot{W}$, *Z, g* and $\dot{Q}$ are the mass flow rate, enthalpy, velocity, power, height, gravitational acceleration, and heat transfer rate, respectively.

2.2.1. Steam/water line

The gasification reaction is as follows [41, 42]:

$$CH_aO_bN_c + wH_2O + m\,(O_2 + 3.76N_2) \rightarrow n_{H_2}H_2 + n_{CO}CO + n_{CO_2}\,CO_2 + n_{H_2O}\,H_2O + n_{CH_4}\,CH_4 + n_{N_2}N_2 \tag{3}$$

$C\,H_aO_bN_c$ represents the biomass general chemical formula. The *a, b, c* coefficients depict the stoichiometric content of *H, O,* and *N* in the biomass. *w* and m denote the moisture and air content. Regarding the mass balance in equation 1 for *C, H, O,* and *N,* the following relations can be written [41, 42]:

$$n_{CO} + n_{CO_2} + n_{CH_4} = 1 \tag{4}$$

$$2n_{H_2} + 2n_{H_2O} + 4n_{CH_4} = a + 2w \tag{5}$$

$$n_{CO} + 2n_{CO_2} + n_{H_2O} = b + w + 2m \tag{6}$$

$$2n_{N_2} = c + 7.52m \quad (7)$$

197

198 Also, the following equilibrium reactions should be taken into account [41, 42]:

199 $$C + 2H_2 \leftrightarrow CH_4 \qquad K = \frac{n_{CH_4} n_{tot}}{(n_{H_2})^2} \left(\frac{P_g}{P_o}\right) = \exp\left(\frac{-\Delta G}{R_u T_{gasifier}}\right) \quad (8)$$

200 $$CO + H_2O \leftrightarrow CO_2 + H_2 \qquad K = \frac{n_{CO_2}\, n_{H_2}}{n_{CO}\, n_{H_2O}} = \exp\left(\frac{-\Delta G}{R_u T_{gasifier}}\right) \quad (9)$$

201 P, T, ΔG, R_u are the pressure, temperature, changes in the Gibbs free energy, and global gas constant.

202 The combustion reaction in the boiler can be written as [43]:

$$\frac{1}{r_a} C_{x1} H_{y1} O_{z1} + \left(x_{o_2} O_2 + x_{N_2} N_2\right) \rightarrow y_{CO_2} CO_2 + y_{N_2} N_2 + y_{o_2} O_2 + y_{H_2O} H_2O \quad (10)$$

$$y_{CO_2} = \frac{x_1}{r_a} \quad (11)$$

$$y_{N_2} = x_{N_2} \quad (12)$$

$$y_{H_2O} = x_{H_2O} + \frac{y_1}{2r_a} \quad (13)$$

$$y_{O_2} = z_1 + x_{O_2} - \frac{x_1}{r_a} - \frac{y_1}{4r_a} \quad (14)$$

$$r_a = \frac{n_{Air}}{n_{SG}} \quad (15)$$

203

204 x_i and y_i are the mass and mole fractions of *i*. r_a specifies the ratio of air/syngas. SG stands for the syngas.

205 In the water/steam line, the mass and energy balance relations for each component are listed in Table 1.

206 Table 1. The mass and energy balance correlations for each component in the water/steam line

No.	Component	Mass balance	Energy balance
1	HW	$\dot{m}_5 = \dot{m}_6$ $\dot{m}_3 = \dot{m}_4$	$\dot{m}_3(h_3 - h_4)\eta_{HX} = \dot{m}_5(h_6 - h_5)$
2	P II	$\dot{m}_{23} = \dot{m}_5$	$\dot{W}_{PII} = \dot{m}_5(h_5 - h_{23})$
3	MX	$\dot{m}_{23} = \dot{m}_{11} + \dot{m}_{18}$	$\dot{m}_{23} h_{23} = \dot{m}_{11} h_{11} + \dot{m}_{18} h_{18}$

207

208 In this table, HW and MX mean water heater and mixer, respectively.

209 ***2.2.2. CO_2 cycle/LNG heat sink***

The mass and energy balance equations for the CO_2 cycle and LNG line are brought in Table 2.

Table 2. The mass and energy balance equations for the CO_2 cycle and LNG line

No.	Component	Mass balance	Energy balance
1	P I	$\dot{m}_{19} = \dot{m}_{20}$	$\dot{W}_{PI} = \eta_P \dot{m}_5 (h_5 - h_{23})$
2	Eva	$\dot{m}_{20} = \dot{m}_{21}$ $\dot{m}_{10} = \dot{m}_{18}$	$\dot{m}_{10}(h_{10} - h_{18})\eta_{HX}$=$\dot{m}_{19}(h_{21} - h_{19})$
3	EXP I	$\dot{m}_{21} = \dot{m}_{22}$	$\dot{W}_{EXPI} = \eta_{EXP} \dot{m}_{21}(h_{21} - h_{22})$
4	Cond	$\dot{m}_{22} = \dot{m}_{19}$, $\dot{m}_{24} = \dot{m}_{25}$	$\dot{Q}_{Cond} = \eta_{Cond} \dot{m}_{24}(h_{25} - h_{24})$=$\dot{m}_{19}(h_{22} - h_{19})$
5	EXP II	$\dot{m}_{25} = \dot{m}_{26}$	$\dot{W}_{EXPII} = \eta_{EXP} \dot{m}_{25}(h_{25} - h_{26})$
6	Cooler	$\dot{m}_{26} = \dot{m}_{27}$	$\dot{Q}_{Cooler}$=$\dot{m}_{26}(h_{26} - h_{27})$

In Table 2, Eva and Cond mean evaporator and condenser.

2.2.3. Multi-effect distillation (MED)

The effect temperature difference is calculated by the following relation [44]:

$$T_i - T_{i-1} = \Delta T == \frac{T_1 - T_N}{N - 1} \tag{16}$$

N and *T* are the effects number and temperature. The subscript *i* denotes the effect number.

The vapor temperature in effects is calculated by [45]:

$$T_{vi} = T_i - BPE \tag{17}$$

Subscript *v* denotes vapor. Boiling point elevation *(BPE)* is defined as a parameter for determining the effect of salt on evaporation temperature [45].

Considering the non-equilibrium allowance (NEA), the flash box temperature can be calculated by [46]:

$$T_{i'} = T_{vi} + NEA \tag{18}$$

where *NEA* is calculated by [46]:

$$NEA = \frac{0.33(T_{vi-1} - T_{vi})}{T_{vi}} \tag{19}$$

The mass concentration and energy balance equations for each effect can be calculated by [47, 48]:

$$\dot{m}_{DW,i} = \dot{m}_{BW,i-1} + \dot{m}_{SW,i} - \dot{m}_{BW,i} \tag{20}$$

$$\dot{m}_{SW,i}x_{SW,i} + \dot{m}_{BW,i-1}x_{BW,i-1} = \dot{m}_{BW,i}x_{BW,i} \tag{21}$$

$$\dot{m}_{DW,i}L_N = \left[\dot{m}_{DW,N-1} + \sum_{I=1}^{N-2}\left(\dot{m}_{DW,r} + \dot{m}_{DW,i}\right)ff - (N-1)\,\dot{m}_{SW,N}\right]L_{N-1} - \dot{m}_{SW}C_P\left(T_N - T_{SW,i}\right) + \dot{m}_{BW,N-1}C_P\Delta T \tag{22}$$

$x, L,$ and ff represent the salt concentration, latent heat, and flashing fraction. Subscript r denotes entrained steam.

The overall surface area of each effect and condenser is calculated by [48, 49]:

$$A_{effects} = \frac{\left[\left(\dot{m}_{DW,N-1} + \cdots + \dot{m}_{DW,N-2} + \dot{m}_{DW,r}\right)ff - (N-1)ff\dot{m}_{SW,N}\right]L_{N-1}}{U_{effects}\left(T_{v,N-1} - T_N\right)} \tag{23}$$

$$A_{cond} = \frac{\left[\left(\dot{m}_{SW} + (\dot{m}_{DW,r}\dot{m}_{DW,1} + \cdots + \dot{m}_{DW,N-1}\right)ff\right]L_N}{U_{cond}LMTD_{cond}} \tag{24}$$

LMTD and U denote logarithmic mean temperature difference and overall heat transfer coefficient. Subscript cond denotes condenser.

U for the effects and condenser can be calculated by the following relations [48, 49]:

$$U_{effects} = 1939.4 + 1.40562T_{effect} - 2.07525 \times 10^{-2}{T_{effect}}^2 + 2.3186 \times 10^{-3}{T_{effect}}^3 \tag{25}$$

$$U_{cond} = 1617.5 + 0.1537T_{cond} - 0.1825{T_{cond}}^2 + 8.026 \times 10^{-5}{T_{cond}}^3 \tag{26}$$

The recovery ratio (*RR*) and gained output ratio (*GOR*) of the MED can be calculated by the following relations [48, 49]:

$$RR = \frac{\dot{m}_{DW}}{\dot{m}_{SW}} \quad (27)$$

$$GOR = \frac{\dot{m}_{DW}}{\dot{m}_{9}} \quad (28)$$

237

238 ***2.2.4.*** **Electrodialysis (*ELECD)***

239 ELECD is a system to convert the B to NaOH and HCl. This system consumes electricity. In the ELECD, the
240 following reaction can be considered [50]:

$$NaCl + H_2O \rightarrow NaOH{+}HCl \quad (29)$$

241 The minimum salt concentration for using this system is 26%. This system needs 0.73 kWh/kg NaOH of
242 electrical energy [50].

243 ***2.2.5. System energy efficiency***

244 The CO_2 cycle and system energy efficiencies (ENE) are calculated by the following relations:

$$\eta_{CO2\ cycle} = \frac{\dot{W}_{net,CO2\ cycle}}{\dot{m}_1(h_{10} - h_{18})} \quad (30)$$

$$\eta_{Sys} = \frac{\dot{W}_{net,Sys} + \dot{Q}_{Cooler} + \dot{m}_{15}h_{15} + \dot{m}_{16}h_{16} + \dot{m}_{13}h_{13}}{\dot{m}_1 LHV + \dot{m}_{24}(h_{24} - h_{27})} \quad (31)$$

245

246 In which, $\dot{W}_{net,CO2\ cycle}$ and $\dot{W}_{net,Sys}$ are calculated by the following relations:

$$\dot{W}_{net,CO2\ cycle} = \dot{W}_{EXPI} - \dot{W}_{PI} \quad (32)$$

$$\dot{W}_{net,Sys} = \dot{W}_{EXPI} - \dot{W}_{PI} + \dot{W}_{EXPII} - \dot{W}_{PII} - \dot{W}_{ELECD} \quad (33)$$

247

248 **2.3. Exergy assessment *and system exergy efficiency***

249 Specific exergy is classified into four categories denoted as chemical, kinetic, physical, and potential as
250 noticed below [51, 52]:

$$\Psi = \sum x_i \Psi_{chi} + \frac{V^2}{2} + gz + (h - h_0) - T_0(s - s_0) + T_0 \sum x_i R_i \ln y_i \quad (34)$$

251

Ψ and *x* denote specific exergy and mass fraction. g, *z,* and *V* are acceleration of gravity, velocity, and height. s and y depict specific entropy and mole fraction. ch, 0, and i are chemicals, standard conditions, and species. Table 3 presents the exergy destruction rate (EDR) for all equipment of the MGS.

Table 3. The EDR for all system components

No.	Component	EDR (kW)
1	Cooler	$\dot{m}_{26}\Psi_{26} - \dot{Q}_{Cooler}(1-\frac{T_{26}}{T_0}) - \dot{m}_{27}\Psi_{27}$
2	EXP II	$\dot{m}_{25}e_{25} - \dot{m}_{26}e_{26} - \dot{W}_{EXPII}$
3	Cond	$\dot{m}_{22}\Psi_{22} - \dot{m}_{19}\Psi_{19} + \dot{m}_{24}\Psi_{24} - \dot{m}_{25}\Psi_{25}$
4	EXP I	$\dot{m}_{21}e_{21} - \dot{m}_{22}e_{22} - \dot{W}_{EXPI}$
5	Eva	$\dot{m}_{20}\Psi_{20} - \dot{m}_{21}\Psi_{21} + \dot{m}_{10}\Psi_{10} - \dot{m}_{18}\Psi_{18}$
6	P I	$\dot{m}_{19}\Psi_{19} - \dot{m}_{20}\Psi_{20} + \dot{W}_{PI}$
7	Gasifier	$\dot{m}_1\Psi_1 + \dot{m}_2\Psi_2 - \dot{m}_3\Psi_3$
8	MED	$\dot{m}_9\Psi_9 + \dot{m}_{12}\Psi_{12} - \dot{m}_{10}\Psi_{10} - \dot{m}_{13}\Psi_{13} - \dot{m}_{14}\Psi_{14}$
9	ELECD	$\dot{m}_{14}\Psi_{14} + \dot{W}_{ELECD} - \dot{m}_{15}\Psi_{15} - \dot{m}_{16}\Psi_{16}$
10	P II	$\dot{m}_{23}\Psi_{23} - \dot{m}_5\Psi_5 + \dot{W}_{PII}$
11	Heater	$\dot{m}_3\Psi_3 - \dot{m}_4\Psi_4 + \dot{m}_5\Psi_5 - \dot{m}_6\Psi_6$
12	MX	$\dot{m}_{11}\Psi_{11} + \dot{m}_{18}\Psi_{18} - \dot{m}_{23}\Psi_{23}$
13	Boiler	$\dot{m}_4\Psi_4 - \dot{m}_7\Psi_7 - \dot{m}_8\Psi_8 + \dot{m}_6\Psi_6$

The CO_2 cycle and system exergy efficiencies (EXE) are calculated by the following relations:

$$\varepsilon_{CO2\ cycle} = \frac{\dot{W}_{net,CO2\ cycle}}{\dot{m}_1(\Psi_{10} - \Psi_{18})} \tag{35}$$

$$\varepsilon_{Sys} = \frac{\dot{W}_{net,Sys} + \dot{Q}_{Cooler}(1-\frac{T_{26}}{T_0}) + \dot{m}_{15}\Psi_{15} + \dot{m}_{16}\Psi_{16} + \dot{m}_{13}\Psi_{13}}{\dot{m}_1 LHV + \dot{m}_{24}(\Psi_{24} - \Psi_{27})} \tag{36}$$

The biomass chemical exergy can be calculated by [53]:

$$\Psi_{ch} = \beta(LHV + \omega h_{fg}) \quad (37)$$

$$\beta = \frac{1.0439 + 0.1882(H/C) - 0.2509\big(1 + 0.7256(H/C)\big) + 0.0383(N/C)}{1 - 0.3035(N/C)} \quad (38)$$

h_{fg} denotes the enthalpy of vaporization.

2.4. Economic evaluation

The annual income (AI) of the MGS is calculated by selling the products annually and it is calculated by the following relation [54, 55]:

$$AI = Y_{elec}c_{elec} + Y_{cooling}c_{cooling} + Y_{DW}c_{DW} + Y_{NaOH}c_{NaOH} + Y_{HCl}c_{HCl} \quad (39)$$

c and Y represent products specific costs and annual products (Table 4). Subscript elec denotes electricity.

Table 4. The specific cost of fuel and products

No.	Specific cost of products and fuel	Unit	Value	Ref.
Products				
1	Electricity	$/kWh	0.12	[56]
2	Cooling	$/kWh	0.06	[57]
3	Demineralized water	$/m^3	5.8	[58]
4	Sodium hydroxide	$/kg	0.74	[59]
5	Hydrochloric Acid	$/kg	0.35	[60]
6	LNG	$/kg	0.009	[61]

The purchased equipment cost (PEC) for all components is depicted in Table 5.

Table 5. PEC for all components

No	Component		PEC ($)	Ref
1	**P I**		$10^{3.3892+0.05361logW+0.1538(logW_P)^2}$	[23]
2	**Eva**		$(A/0.093)^{0.78}$	[23]
3	**EXP I**		$10^{2.6259+1.43981logW_{EXP}-0.1776(logW_{EXP})^2}$	[23]
4	**Cond**		$(A/0.093)^{0.78}$	[23]
5	**EXP II**		$479.34\left(\frac{\dot{m}_8}{0.93-\eta_{EXP}}\right)\ln(\frac{P_8}{P_9})(1-\exp(0.036T_8-54.4))$	[57]
6	**Cooler**		$1.218\times\exp(0.4692+0.1203\ln(\dot{Q}_{Cooler})+0.0931(\ln(\dot{Q}_{Cooler}))^2)$	[58]
7	**Boiler**		$283\dot{Q}_{in}$	[62]
8	**Gasifier**		$1600\ (3600\dot{m}_1)^{0.67}$	[63]
9	**Heater**		$8500+409A^{0.85}$	[64]
10	**P II**		$3540(\dot{W}_P)^{0.71}$	[65]
11	**MED**	**Effects**	$201.67\dot{Q}\times LMTD^{-1}dp_{SW}^{0.15}dp_s^{-0.15}$	[66]
12		**Condenser**	$430\times0.582\times\dot{Q}LMTD^{-1}dp_{SW}^{0.01}dp_s^{-0.1}$	[66]
13	**ELECD**		$1000\ \dot{W}_{ELECD}$	[50]

For estimating the surface area of the *HX*, the logarithmic method is used and the following relation is considered [67]:

$$\dot{Q}=UAF_t\Delta T_{In} \quad (40)$$

Where U, $\dot{Q}$, A, F_t, and ΔT_{In} are the overall heat transfer coefficient, heat transfer rate, surface area, correction factor, and logarithmic mean temperature difference. The overall heat transfer coefficient for HX is considered to be 700 W/m^{2}K.

According to ref [68], total capital investment (*TCI*) is classified into three types. They are direct cost (*DC*), indirect cost (*IC*), and other costs (*OC*). Table 6 shows the components of *DC*, *IC*, and *OC* as a percentage of the *PEC*.

Table 6. The components of *DC, IC*, and *OC* as a percentage of the *PEC*

No.	Items	Percentage
1	Piping (PI)	10
2	Instrumentation and controls (I&C)	6
3	Electrical equipment and materials (E)	10
4	Land (L)	4
5	Civil, structural, and architectural work (CSA)	17
6	Service facilities (SF)	34
7	Engineering and supervision (E&S)	25
8	Construction costs including contractor's profit	30
9	Contingencies	24
10	Startup costs (S&C)	9
11	Working capital (WC)	17

The inflation rate effect on the *TCI* is calculated by [69]:

$$TCI_n = TCI_0(1+i)^n \tag{41}$$

n and *i* depict the years' number and the rate of inflation (3.1%) [70]. Operation and maintenance cost (*OMC*) is considered to be 3% of the *TCI* [54, 55].

Thus, the total cost (*TC*) is calculated as follows [68]:

$$TC \quad = TCI_n + OMC \tag{42}$$

The simple payback period (Z_S) index is calculated by [54, 55]:

$$Z_S = \frac{TC}{AI} \tag{43}$$

The payback period (Z_P) index can be obtained by [54, 55]:

$$Z_P = \frac{ln(\frac{AI}{AI - r.\mathrm{TC}})}{ln(1+r)} \tag{44}$$

r depicts the discount factor (3%) [54, 55].

The net present value (*NPV*) is calculated by the following relation [54, 55]:

$$Z_N = AI\frac{(1+r)^N - 1}{r(1+r)^N} - \mathrm{TC} \tag{45}$$

N refers to the life cycle of the project (25 years) [68]. The Internal rate of return *(Z_{IR})* can be obtained as follows [54, 55, 71]:

$$Z_{IR} = \frac{AI}{\mathrm{TC}}\left[1 - \frac{1}{(1+IRR)^N}\right] \tag{46}$$

3) Results and discussion

For the MGS investigation, a computational program is developed in the engineering equation solver (EES). The thermodynamic properties of all working fluids are considered via the external library of EES. The input data of the computational program is brought in Table 7. The biomass used in the gasifier is Alfalfa with the $CH_{1.324}O_{0.594}N_{0.063}$ chemical formula, a molecular weight of 23.68 kg/kmole, and LHV of 12233.8 kJ/kg [72, 73]. The flowchart of the computer code is depicted in Figure 4.

322 Table 7. Input data of system modeling

No.	Parameter	Definition	Unit	Values
1	T_{24}	LNG temperature	^{o}C	T_{19}-10
2	P_{25}	Outlet EXP II pressure	kPa	121.6
3	$\dot{m}_1$	Working fluid mass flow rate in CO_2 cycle	kg/s	10
4	w	Moisture ratio in biomass	-	0.34
5	TBT	Top brine temperature	^{o}C	66.3
6	BBT	Bottom brine temperature	^{o}C	40
7	x_{12}	Seawater salt concentration	-	35
8	x_{14}	Brine salt concentration	-	60
9	m	Equ 3	-	0.187
10	N	Number of effects	-	4
11	T_{25}	Inlet EXP II temperature	^{o}C	25
12	P_{24}	LNG tank pressure	kPa	658.5
13	P_{22}	Condenser pressure in CO_2 cycle	kPa	607.8
14	P_{21}	Evaporator pressure in CO_2 cycle	kPa	1519.5
15	r_a	Air/fuel ratio in boiler	-	2.1
16	T_4	Syngas outlet temperature from heater	^{o}C	85
17	T_6	Water outlet temperature from heater	^{o}C	75

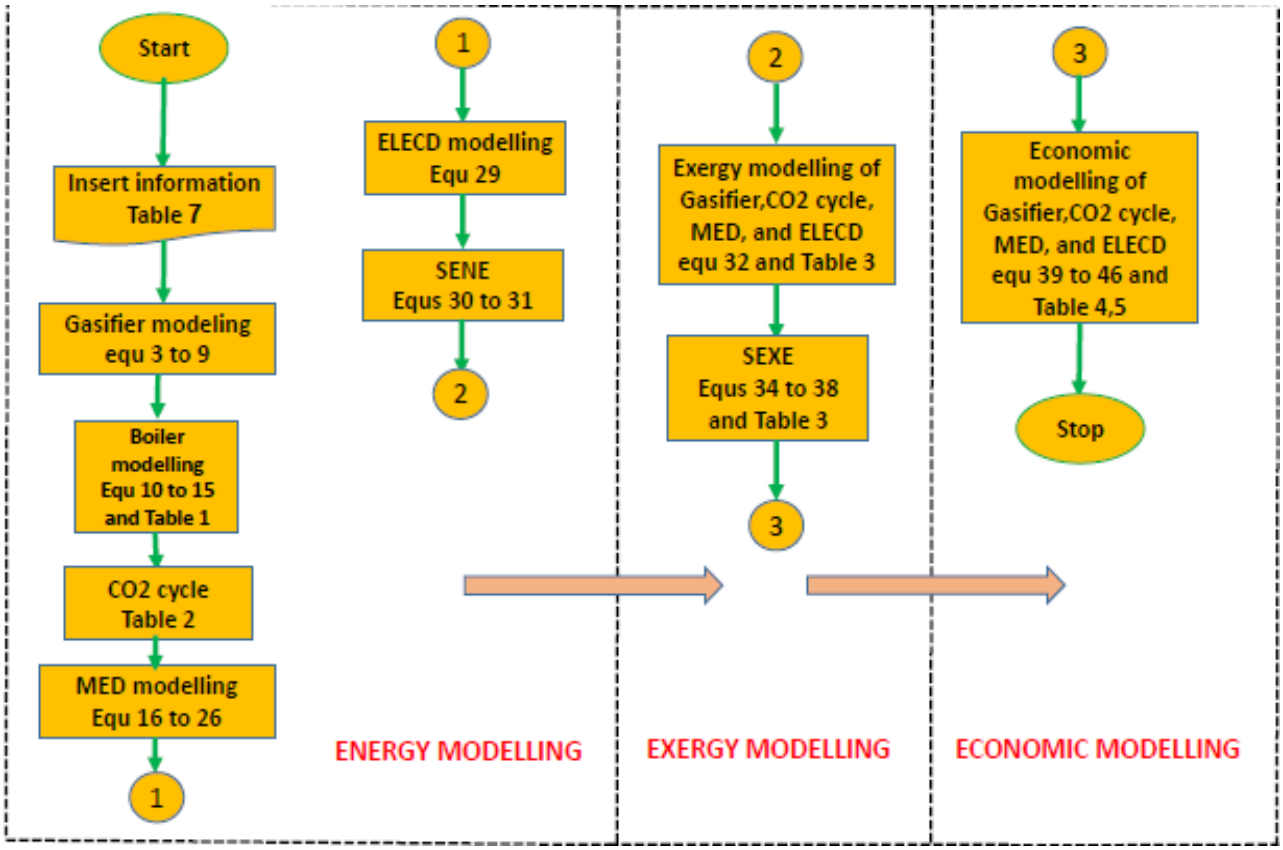

Figure 4. Flowchart of the computer code

3.1. Model validation

Validation of model results is essential to use the research results in the related industry or further research. In this work, the configuration of the proposed system is novel. So, validation of the whole system is not feasible and each sub-system was validated individually.

The data from ref [72] is considered for the gasifier. The considered biomass feed type is bean straw with 0.1294 kg/s mass flow rate and 0.0006 kmole/kmole intake air to biomass ratio. The gasifier products predicted by the computer model and ref [72] are shown in Figure 5, confirming the good agreement. For the MED validation, ref [74] is considered. Table 8 depicts the results of the comparison, which also validates the model. The ref [75] is considered to validate the CO_2 cycle with the LNG heat sink. The CO_2 and LNG turbines' power production and pumps power consumption are compared. Table 9 shows a comparison between the present work and reference [75]. From these comparisons, it can be concluded that the computer model provides reliable data.

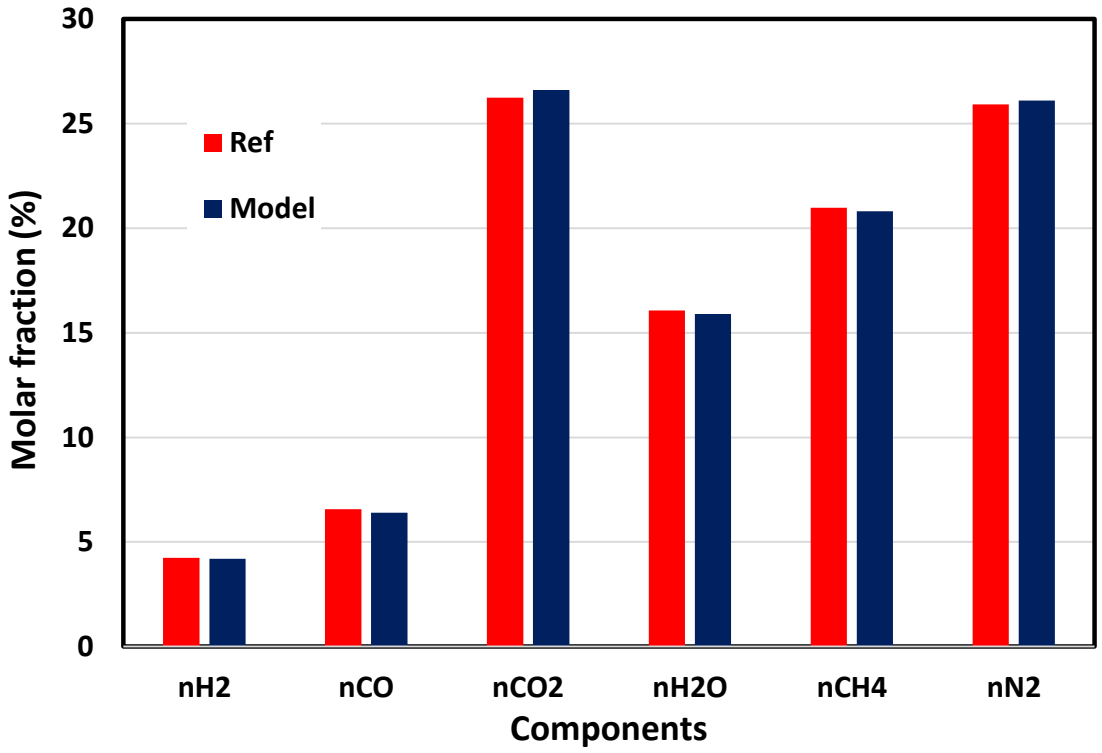

Figure 5. The comparison between gasifier products of the computer model and ref. [72]

Table 8. The compared results of the generated model and ref. [74] for the MED validation

No.	Parameter	Unit	Model	Ref [74]	Error (%)
1	$\dot{m}_{13}$	kg/s	0.802	0.8125	1.6
2	$\dot{m}_{14}$	kg/s	0.056	0.055	1.8
3	GOR	-	9.2	9.4012	2.1

Table 9. Comparison between the model and ref. [75] for the CO_2 cycle

No.	Parameters	Unit	Model	Ref [75]	Error (%)
1	$\dot{W}_{EXP\ I}$	kW	14.2	14.66	3.1
2	$\dot{W}_{PI}$	kW	4.98	4.778	4.2
3	$\dot{W}_{EXP\ II}$	kW	7.19	7.464	3.6
4	$\dot{W}_{P\ II}$	kW	3.81	3.693	3.1

3.2. Energy and exergy assessment results

The thermodynamic characteristics of all MGS streams, such as mass flow rate, pressure, temperature, specific enthalpy, and specific exergy, are reported in Table 10. The MED specification is summarized in Table 11. The electrical power production and consumption for various components and the cooling production of the MGS are shown in Table 12. It seems that the expander (EXP II) in the LNG line produces more electrical power than the expander in the CO_2 cycle due to high pressure of NG after exchanging heat with the condenser of the CO_2 cycle. The products of the system are shown in Table 13. The MGS products are 73.17 GWh of cooling, 103 GWh of electrical energy, 1223 Ton of NaOH, 1114 Ton of HCl, and 212.6 m^3 of PW annually. This system consumes 17130.2 Ton/year of Alfalfa biomass. The calculated ratio of cooling to power is 71%.

Table 10. The thermodynamic characteristics of all MGS streams

No	ṁ (kg/s)	P (kPa)	T(°C)	h (J/kg)	e (J/kg)
1	0.5948	101.3	10	16300.0	11890000.0
2	0.6476	101.3	10	283507.0	6692.0
3	1.242	202.6	430.8	642994.0	5551000.0
4	1.242	192.6	85	126876.0	5149000.0
5	4.399	121.6	32.5	136240.0	3580.0
6	4.399	121.6	75	314025.0	69086.0
7	1.353	101.3	480	716477.0	641162.0
8	4.399	101.3	125	2726000.0	607337.0
9	2.2	101.3	125	2726000.0	607337.0
10	2.2	101.3	125	2726000.0	607337.0
11	2.2	101.3	40	167586.0	6213.0
12	112.5	101.3	25	99766.0	1364.0
13	7.384	101.3	39.46	165255.0	5905.0
14	1.034	101.3	313.2	154184.0	7910.0
15	0.03869	101.3	313.2	686848.0	214779.0
16	0.04245	101.3	313.2	686848.0	589373.0
17	9.303	101.3	313.2	154184.0	7910.0
18	2.2	101.3	25	104844.0	1606.0
19	10	607.8	-52.81	-419369.0	199761.0
20	10	1520	-52.46	-418448.0	200504.0
21	10	1520	115	71690.0	155362.0
22	10	607.8	55.15	21267.0	97147.0
23	4.399	101.3	32.5	136215.0	3552.0
24	59.5	658.5	-62.81	-200676.0	297925.0
25	59.5	658.5	48	46196.0	278333.0
26	59.5	101.3	-51.17	-165844.0	66293.0
27	59.5	101.3	20	-12119.0	381.9

Table 11. The MED specification

No.	Variable	Unit	1	2	3	4
1	$A_{effects}$	m^2	13.02	177.4	194.9	210.3
2	BPE	°C	0.417	0.452	0.49	0.538
3	T_b	°C	66.3	57.5	48.8	40
4	T_{dv}	°C	65.9	57.1	48.3	39.5
6	U_{effect}	W/m^2K	6319	2605	2383	2219
7	P	kPa	26.03	17.4	11.3	7.2
8	$A_{condenser}$	m^2	277.7			
8	GOR	-	3.36			
9	RR	-	0.065			

Table 12. The electrical power production and consumption for various components

No.	Items	Unit	Values
1	$\dot{W}_{EXP\ I}$	kW	504.23
2	$\dot{W}_{EXP\ II}$	kW	12490
3	$\dot{W}_{P\ I}$	kW	9.2
4	$\dot{W}_{P\ II}$	kW	0.14
5	$\dot{W}_{ELECD}$	kW	111.5
6	$\dot{Q}_{Cooler}$	kW	9146

Table 13. The products of the system

No.	Products	Unit	Values
1	Electrical energy	GWh	103
2	Cooling energy	GWh	73.17
3	NaOH	Ton/year	1223
4	HCl	Ton/year	1114
5	PW	m^3/year	212.6

Figure 6 shows the energy and exergy efficiencies (ENE and EXE) of the CO_2 cycle and MGS. According to Figure 6, the CO_2 cycle ENE and EXE are 8.5% and 37.1%; however, the MGS ENE and EXE are 75.1% and 88.4%, respectively. So, it can be concluded that the MGS is beneficial from the energy and exergy point

of view. In the CO_2 cycle, the difference between the heat source and sink temperatures is T_{21}-T_{18}, while in the MGS, it is T_7-T_{24}. According to the Carnot efficiency, $((1 - \frac{T_L}{T_H}), T_L \text{ and } T_H: \text{heat sink and source temperatures})$, by increasing heat source and sink temperatures, the efficiency of all engines is improved. Thus, the ENE and EXE of the MGS are improved considerably. In comparison between MGS and CO_2 cycle, the ENE of the MGS is much higher due to the higher number of products than the CO_2 cycle.

The EDR percentage of all MGS sub-systems including CO_2 cycle, steam, LNG lines, MED, and ELECD, is depicted in Figure 7. The highest percentage of EDR belongs to the LNG line due to LNG's high mass flow rate in this line. After the LNG line, the steam line features the most significant percentage of the EDR owing to the high temperature and mass flow rate of steam. 14.7% and 10.4% of the EDR are related to the CO_2 cycle and MED. The lowest portion of the EDR is related to ELECD due to the low mass flow rate of brine. In the CO_2 cycle, the evaporator features the biggest portion of the EDR because of heat transfer taking place between steam and CO_2. The P I has the lowest rate of the EDR arising from a slight difference within thermodynamic features in the inlet and outlet of the P I. The EXP I and Cond have 3.9% and 6.97% of EDR percentage. In the steam line, the most distinguished portion of the EDR belongs to the boiler because of burning syngas and changing the water to steam that two important sources of the EDR named heat transfer and combustion reaction. The EDR percentage of the gasifier and heater is similar. The EDR percentage of P II is negligible.

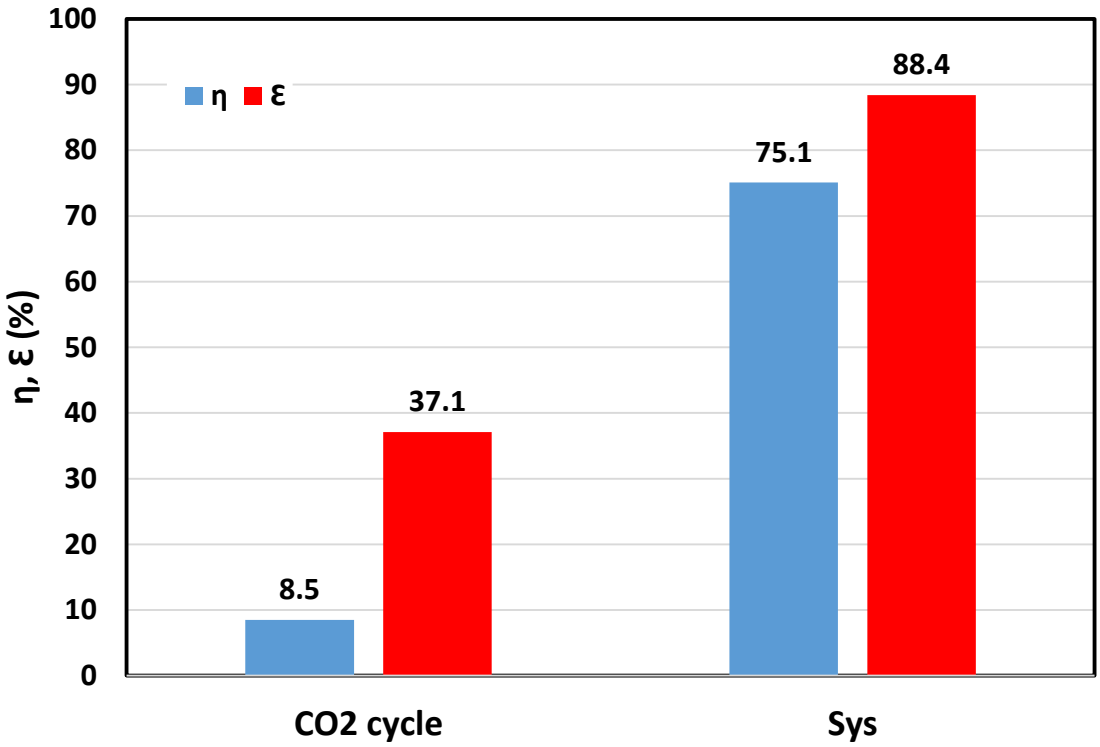

406

407 Figure 6. The energy and exergy efficiencies of the CO_2 cycle and MGS

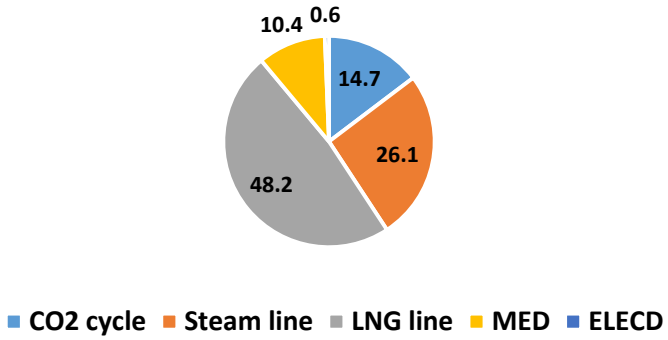

408

409 (a)

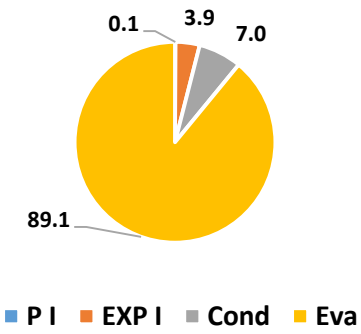

410

411 (b)

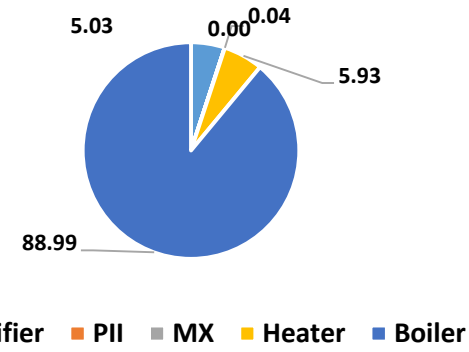

412

413 (c)

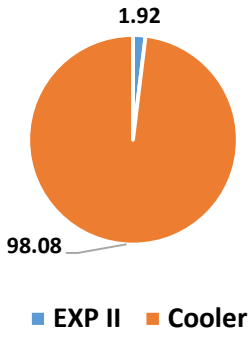

414

415 (d)

416 Figure 7. The exergy destruction rate percentage of MGS sub-systems (a) total system, (b) CO_2 cycle (c)

417 steam line, (d) LNG line

418 **3.3. Economic analysis results**

Figure 8 shows the percentage of AI for all products of the MGS. The highest and lowest percentages of the AI are related to electricity and PW. In addition, cooling represents the second part of the AI. The AI of NaOH is roughly twice the AI of HCl. By considering Tables 5 & 6 and equation 42, TC of the MGS is equal to 7.459×10^{6} $. Considering equations 43 to 46, the SPP, PP, NPV, and IRR are equal to 2.78 years, 2.94 years, 3.929×10^{7} $, and 0.36, respectively.

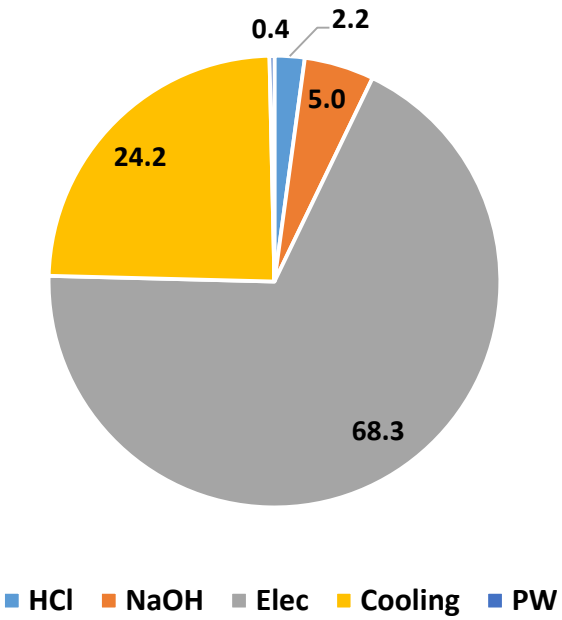

Figure 8. The percentage of the annual income for all products of the MGS

3.4. Parametric study

The variation of the CO_2 cycle ENE and EXE versus polytrophic performance of EXP I ($\eta_{EXP\ I}$) is depicted in Figure 9. If the $\eta_{EXP\ I}$ is doubled (50% to 100%), the ENE and EXE of the CO_2 cycle are also doubled. This trend shows the importance of $\eta_{EXP\ I}$ on the cycle ENE and EXE. Since increasing the $\eta_{EXP\ I}$ has a direct effect on the ENE and EXE of the CO2 cycle.

Figure 10 shows the variation of ENE, EXE, and EDR of the CO_2 cycle versus condenser pressure (P_{22}). Increasing the P_{22} from 600 to 1000 kPa causes reductions in ENE, EXE, and EDR of the CO_2 cycle, since an increase in P_{22} causes a reduction in EXP I power production and P I power consumption. However, reduction in EXP I power production is more than P I power consumption.

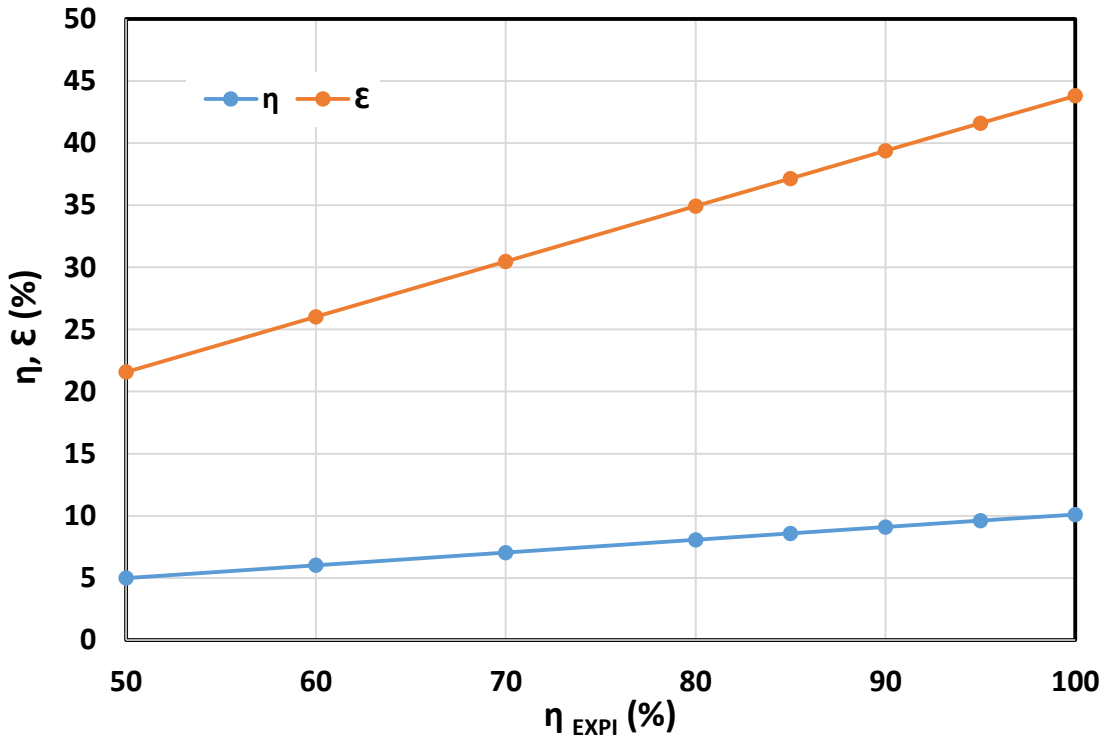

435

436 Figure 9. The variation of the CO_2 cycle energy and exergy efficiencies versus polytrophic performance of
437 EXP I ($\eta_{EXP\ I}$)

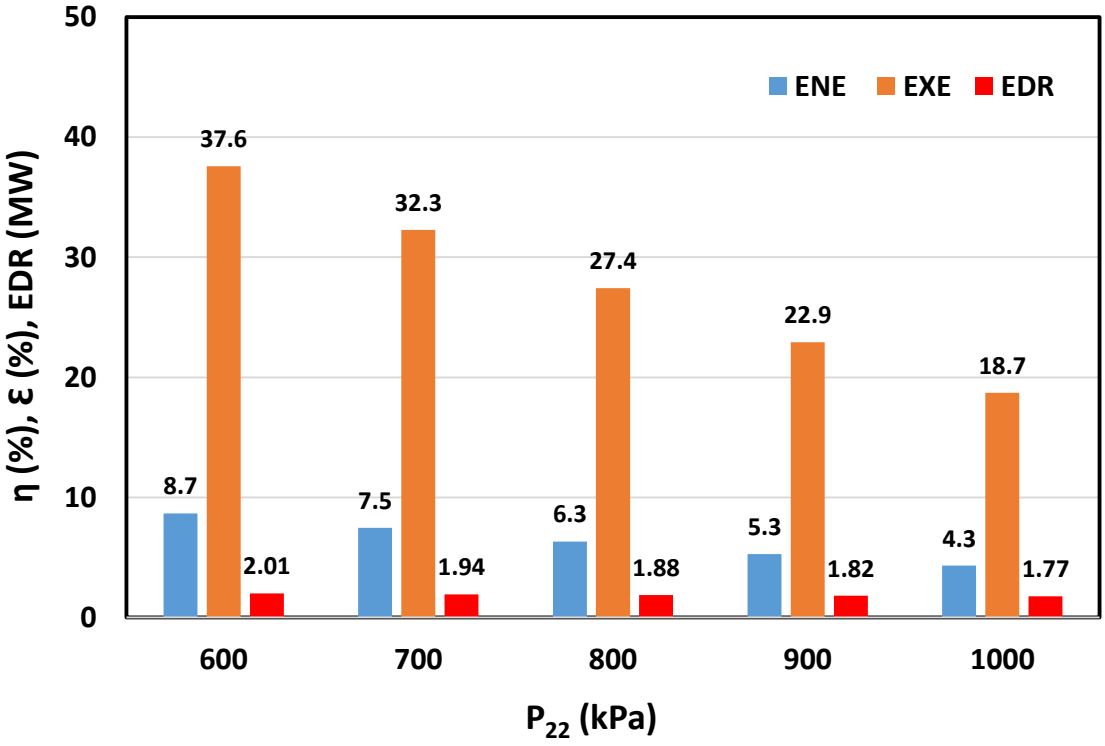

438

Figure 10. The variation of energy and exergy efficiencies, and EDR of the CO_2 cycle versus condenser pressure (P22)

For the parametric study of the gasifier, other types of biomass were taken into account (Table 14). The chemical formula, LHV, and molecular weight of the different biomass types are summarized in this table. The specifications of these biomass types were included in the computer code. Figure 11 displays the ENE and EXE of the MGS that uses these types of biomass. It is clear that with increasing the LHV of the biomasses, both the ENE and EXE of the MGS decrease. It can be concluded that by increasing the LHV of the biomass, the recovery ratio declines.

Table 14. The chemical formula, molecular weight, and LHV for different types of biomass [72, 73]

Cases	Name	Chemical Formula	Molecular weight (kg/kmole)	LHV (kJ/kg)
1	Oats strand	$CH_{1.269}O_{0.626}N_{0.013}$	23.46	12480
2	Rapeseed	$CH_{1.491}O_{0.832}N_{0.011}$	24.95	13084
3	Wheat straw	$CH_{1.434}O_{0.675}N_{0.031}$	24.69	13215.2

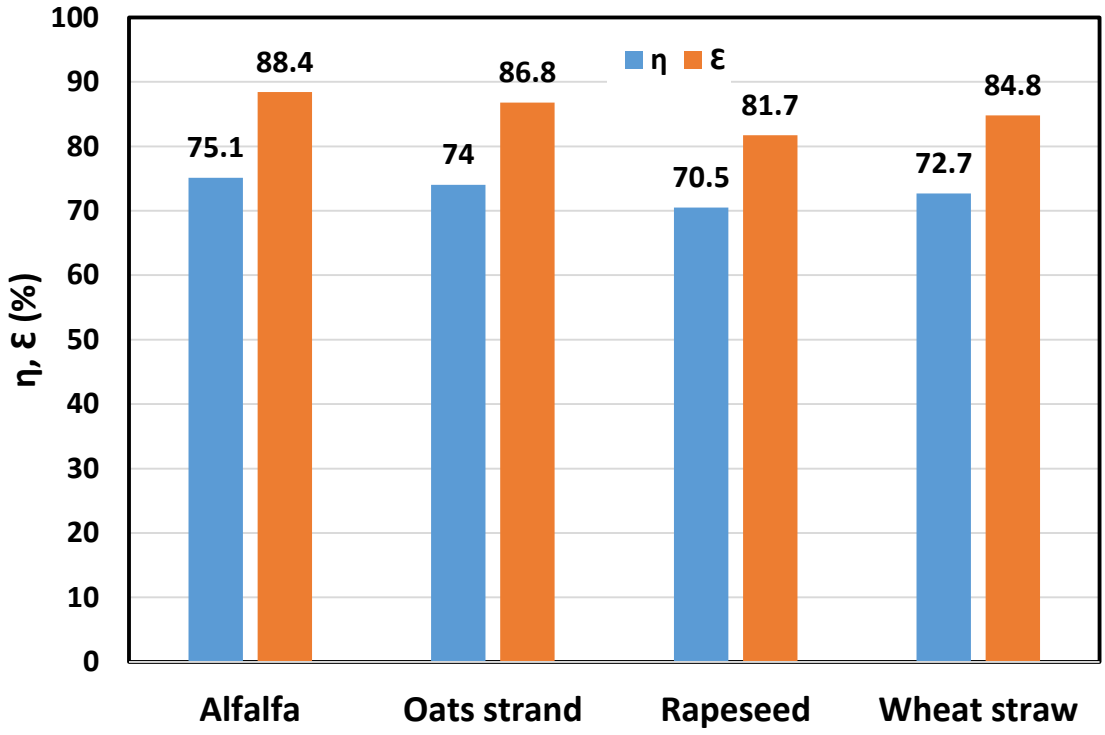

Figure 11. The energy and exergy efficiencies of the MGS that uses different types of biomass

Figure 12 shows the ENE and EXE of the MGS versus moisture content (w) in the biomass. Increasing w causes a reduction in the ENE and EXE of the MGS. Although increasing w favors methane production due

453 to hydrogen in the moisture, it reduces the exhaust temperature of the biogas produced in the gasifier
454 and heat recovered in the heater.

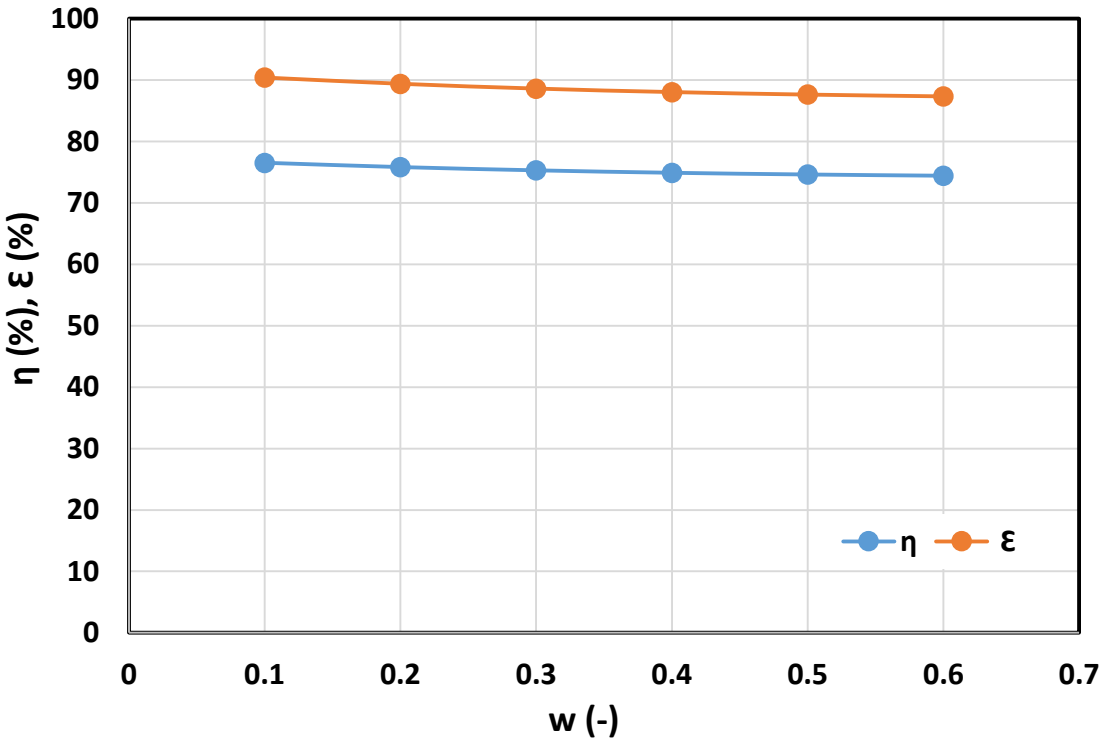

455

456 Figure 12. The energy and exergy efficiencies of the MGS versus moisture content (w) in the biomass

457 Figure 13 shows the variation of DW and B with x_f (salt concentration of seawater). Increasing x_f from 15
458 to 50 causes a reduction in DW mass flow rate while increasing B mass flow rate (although the effect of
459 this increase is more pronounced for B than DW).

460 Figure 14 shows the variation of the GOR of the MED system with x_f. Increasing x_f decreases the GOR of
461 the MED system. By increasing x_f from 15 to 50, the GOR of the MED system decreases by around 12.5%.
462 Since more steam should be consumed to separate salt from the seawater that has a direct effect on
463 system performance.

464

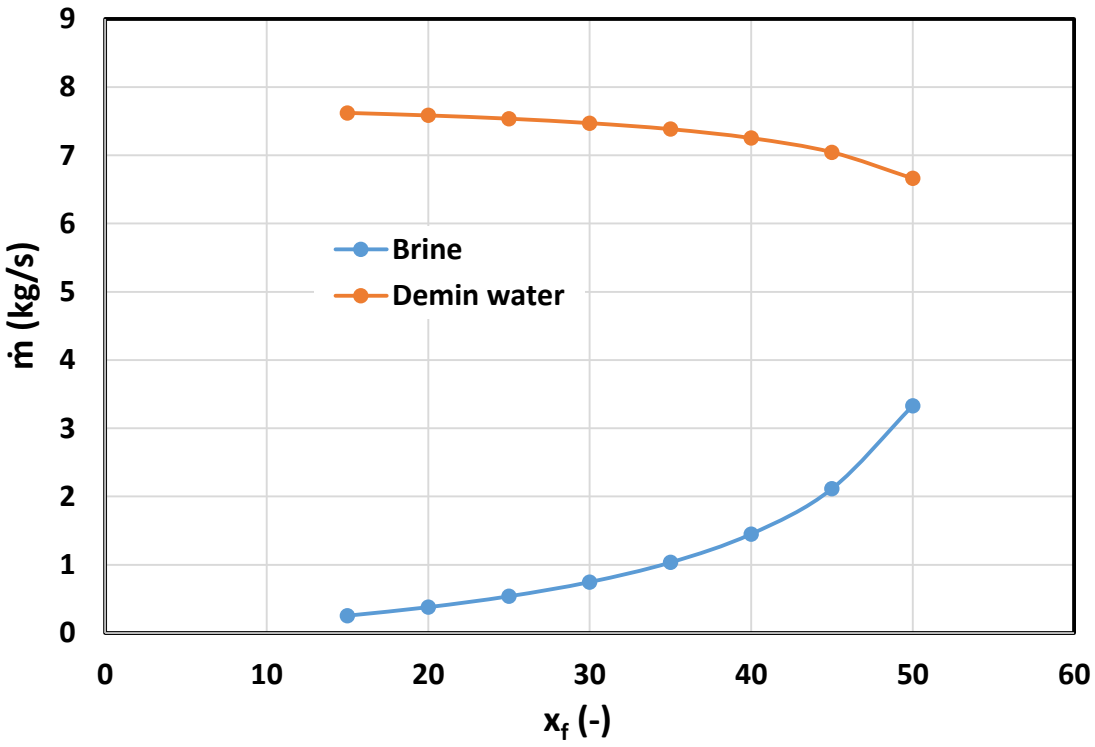

Figure 13. The variation of DW and brine with x_f

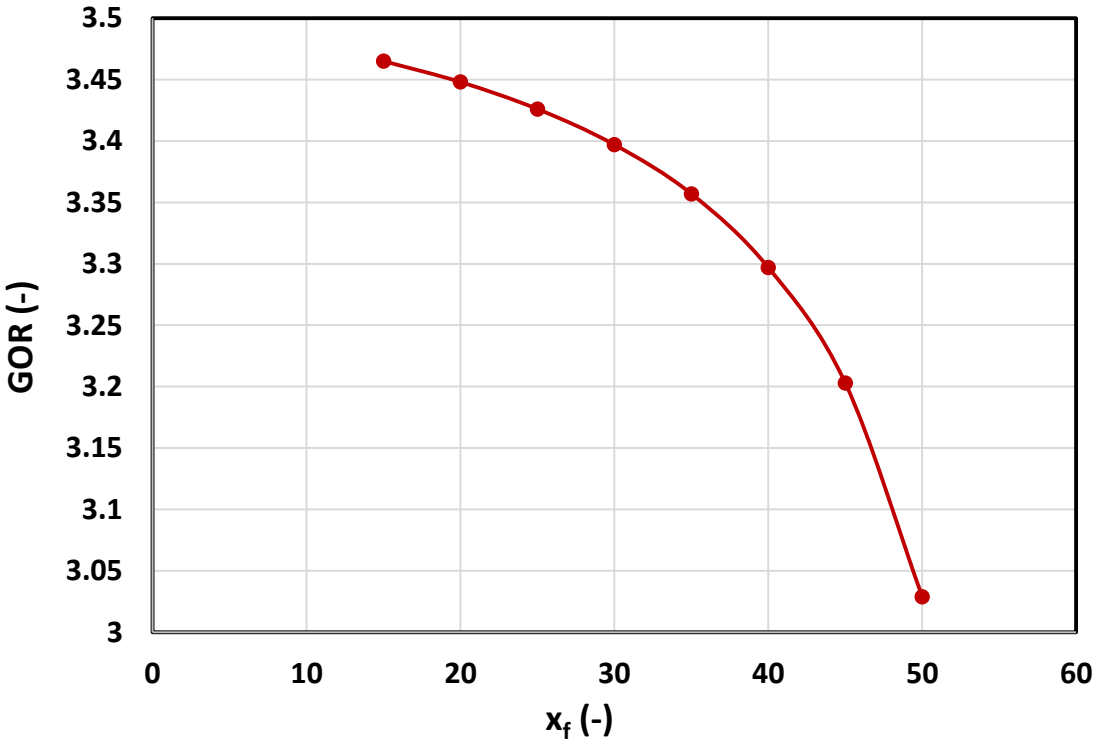

Figure 14. The variation of the GOR of the MED system with x_f

Figure 15 displays the change of PP and SPP against the number of MED effects (N). The slope of both curves is negative in this figure. This means that PW increase due to N increase overcomes the increasing TIC. Hence, the SPP and PP are decreased.

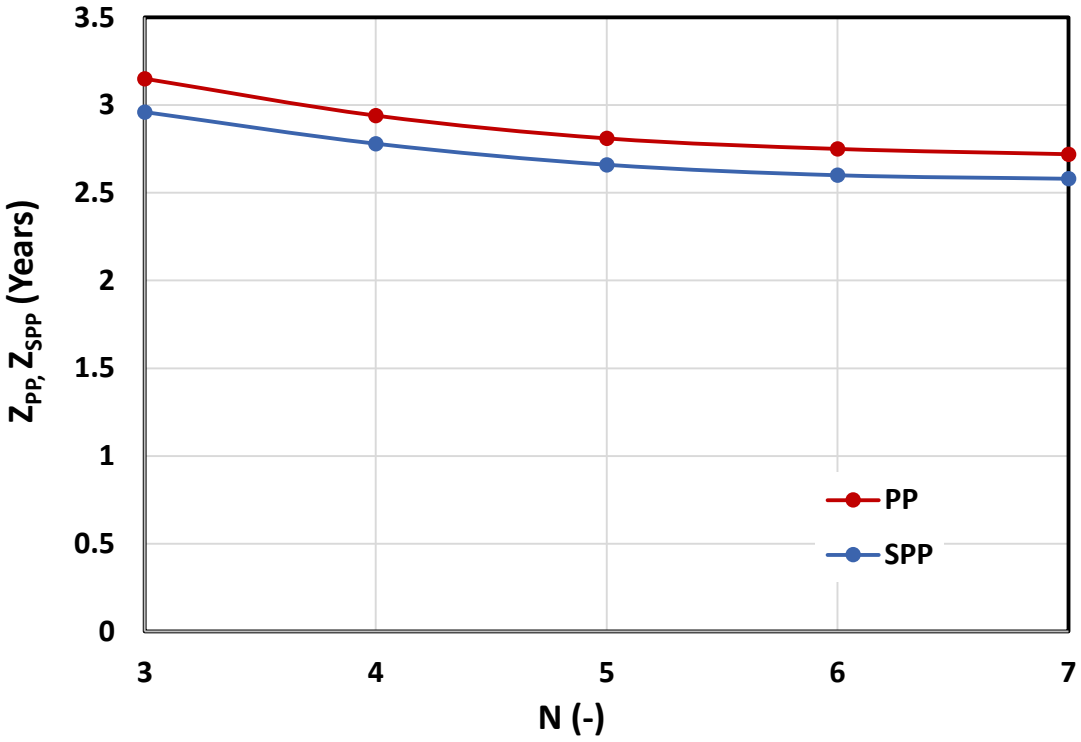

Figure 15. The variation of PP and SPP with number of MED effects (N)

4) Conclusion

Energy, exergy and economic analysis of a novel proposed biomass-based combined cycle was carried out in this research work. In this multigeneration system, biomass provides the needed heat source for boiler operation, LNG line supports cooling production, CO_2 cycle generates power, and multi-effect distillation (MED) system generates distilled water. The electrodialysis (ELECD) is installed downstream of MED to produce sodium hydroxide (NaOH) and hydrogen chloride (HCl), besides avoiding the dissipation of B to the marine ecosystem. The designed integrated system reduces the environmental impact and yields higher productivity. The main achievements of the evaluated configuration are listed thereafter:

- The productions of the proposed MGS include 73.17 GWh of cooling, 103 GWh of electrical energy, 1223 Ton of NaOH, 1114 Ton of HCl, and 212.6 m^3 of PW annually.

- The proposed system consumes 17130.2 Ton/year of Alfalfa biomass. Also, the calculated ratio of cooling to power is 71%.
- The obtained ENE and EXE of modeled MGS are 75.1% and 88.4%, respectively.
- The most significant portion of EDR belongs to the LNG line (mainly owing to the high value of LNG's mass flow rate) and the steam line (mainly because of steam's high mass flow rate and temperature). The lowest percentage of the EDR belongs to the ELECD arising from the low mass flow rate of B.
- The highest and lowest percentages of the AI are relevant to electricity and PW.
- SPP, PP, NPV, and IRR values are obtained at 2.78 years, 2.94 years, 3.929×10^7 \$, and 0.36, respectively.
- Increasing the efficiency of the EXP I from 50% to 100% causes the ENE and EXE of the CO_2 cycle being also doubled.
- With increasing the LHV of the biomasses, the ENE and EXE of the MGS are decreased. It can be concluded that by increasing the LHV of the biomass, the recovery ratio is decreased.
- Increasing biomass moisture content reduces the ENE and EXE of the MGS.
- Increasing the salt concentration of seawater from 15 to 50 leads to a reduction in DW mass flow rate while rising B mass flow rate, and further decreases the GOR of the MED system by around 12.5%.
- The SPP and PP decrease when raising the number of MED effects.

For future development of this MGS, the researches should concentrated on the power consumption of ELECD that all of dissipated brine can be converted to beneficial products and it does not harm the environment.

Nomenclature

Abbreviations

B	Brine
CCHP	Combined cooling, heat, and power
Cond	Condenser

DEABC	Double effect absorption chiller
DV	Distillate vapor
DW	Distilled water
EDR	Exergy destruction rate
Elec	Electrical
ELECD	Electrodialysis
ENE	Energy efficiency
ERC	Ejector refrigeration cycle
EXE	Exergy efficiency
EXP	Expander
G	Generator
GHG	Greenhouse gas
GT	Gas turbine
HW	Heat water
LCOE	Levelized cost of energy
LMTD	Logarithmic mean temperature difference
LNG	Liquefied natural gas
MED	Multi-effect distillation
MGS	Multigeneration system
MOGA	Multi-objective genetic algorithm
MSF	Multi-stage flash
MX	Mixer
NEA	Non-equilibrium allowance

NG	Natural gas
NSGA II	Non-dominated sorting genetic algorithm II
P	Pump
RO	Reverse osmosis
SG	Syngas
SOFC	Solid oxide fuel cell
SW	Seawater
TES	Thermal desalination system
TVC	Thermal vapor compressor

Symbols

A	Surface area (m^2)
AI	Annual income ($)
BPE	Boiling point elevation (^oC)
c	Specific cost of products ($/kWh) or ($/kg) or ($/$m^3$)
CSA	Civil, structural, and architectural work costs ($)
DC	Direct cost ($)
E	Electrical equipment and materials cost ($)
E&S	Engineering and supervision cost ($)
F_t	Correction factor (-)
ff	Flashing fraction (-)
g	Gravitational acceleration (m/s^2)
G	Gibbs function (kJ/kg)
GOR	Gained output ratio (-)

h	Specific enthalpy (kJ/kg)
i	Inflation rate (-)
IC	Indirect cost ($)
I&C	Instrumentation and controls cost ($)
IRR	Internal rate of return (-)
K	Equilibrium constant (-)
L	Latent heat (kJ/kg) or cost of land ($)
LHV	Lower heating value (kJ/kg)
$\dot{m}$	Mass flow rate (kg/s)
N	Number of effects (-)
N	Lifetime of the project (years)
n	Number of years (-)
NEA	Non-equilibrium allowance (^{o}C)
OC	Other costs ($)
OMC	Operation and maintenance cost ($)
P	Pressure (kPa)
PEC	Purchased equipment cost ($)
PEI	Purchased-equipment installation ($)
PI	Piping ($)
PP	Payback period (years)
$\dot{Q}$	Heat transfer rate (kW)
Ru	Universal gas constant, R=8.314 (kJ/kmol.K)
r	Discount factor (-)

r_a	Air-to-fuel ratio (-)
RR	Recovery ratio (-)
s	Specific entropy (kJ/kg.K)
S&C	Startup costs ($)
SF	Service facilities cost ($)
T	Temperature (^oC or K)
TC	Total cost ($)
TCI	Total capital investment ($)
U	Overall heat transfer coefficient (W/m^2K)
V	Velocity (m/s)
WC	Working capital cost ($)
$\dot{W}$	Rate of work transfer (kW)
x	Salt concentration (-)
x	Mass fraction (-)
y	Mole fraction (-)
Y	Yearly capacity (kWh/year) or (kg/year) or (m3/year)
z	Height (m)

Greek symbols

β	Correction factor (-)
η	Energy efficiency (-)
ε	Exergy efficiency (-)
Ψ	Specific exergy (kJ/kg)

Subscripts

0	Dead state
B	Brain
ch	Chemical
cond	Condenser
DV	Distillate vapor
DW	Distilled water
elec	Electrical
ELECD	Electrodialysis
EXP	Expander
HX	Heat exchanger
i	Species, Inlet flow
N	Effects number
P	Pump
s	Steam
SW	Seawater
v	Vapor

510

511

512 **References:**

513 [1] Y. Subramaniam, T.A. Masron, N.H.N. Azman. Biofuels, environmental sustainability, and food
514 security: A review of 51 countries. Energy Research & Social Science. 68 (2020) 101549.
515 [2] S. Abanades, H. Abbaspour, A. Ahmadi, B. Das, M.A. Ehyaei, F. Esmaeilion, et al. A critical review of
516 biogas production and usage with legislations framework across the globe. International Journal of
517 Environmental Science and Technology. (2021).
518 [3] G. Rajaei, F. Atabi, M. Ehyaei. Feasibility of using biogas in a micro turbine for supplying heating,
519 cooling and electricity for a small rural building. Advances in energy research. 5 (2017) 129.

[4] F. Gallucci, H. Hamers, M. Van Zanten, M. van Sint Annaland. Experimental demonstration of chemical-looping combustion of syngas in packed bed reactors with ilmenite. Chemical Engineering Journal. 274 (2015) 156-68.
[5] V.S. Sikarwar, M. Zhao, P.S. Fennell, N. Shah, E.J. Anthony. Progress in biofuel production from gasification. Progress in Energy and Combustion Science. 61 (2017) 189-248.
[6] N. Mir, Y. Bicer. Integration of electrodialysis with renewable energy sources for sustainable freshwater production: A review. Journal of Environmental Management. 289 (2021) 112496.
[7] Ihsanullah. Carbon nanotube membranes for water purification: Developments, challenges, and prospects for the future. Separation and Purification Technology. 209 (2019) 307-37.
[8] M.A. Ehyaei, S. Baloochzadeh, A. Ahmadi, S. Abanades. Energy, exergy, economic, exergoenvironmental, and environmental analyses of a multigeneration system to produce electricity, cooling, potable water, hydrogen and sodium-hypochlorite. Desalination. 501 (2021) 114902.
[9] Y. Cao, M.A. Ehyaei. Energy, exergy, exergoenvironmental, and economic assessments of the multigeneration system powered by geothermal energy. Journal of Cleaner Production. 313 (2021) 127823.
[10] G. Alonso, S. Vargas, E. Del Valle, R. Ramirez. Alternatives of seawater desalination using nuclear power. Nuclear engineering and design. 245 (2012) 39-48.
[11] Y. Wang, N. Lior. Proposal and analysis of a high-efficiency combined desalination and refrigeration system based on the LiBr–H2O absorption cycle—Part 2: Thermal performance analysis and discussions. Energy conversion and management. 52 (2011) 228-35.
[12] D.A. Roberts, E.L. Johnston, N.A. Knott. Impacts of desalination plant discharges on the marine environment: A critical review of published studies. Water research. 44 (2010) 5117-28.
[13] S. van Wyk, A.G. van der Ham, S.R. Kersten. Analysis of the energy consumption of supercritical water desalination (SCWD). Desalination. 474 (2020) 114189.
[14] A. Kumar, K.R. Phillips, G.P. Thiel, U. Schröder, J.H. Lienhard. Direct electrosynthesis of sodium hydroxide and hydrochloric acid from brine streams. Nature Catalysis. 2 (2019) 106-13.
[15] Y. Junjie, S. Shufeng, W. Jinhua, L. Jiping. Improvement of a multi-stage flash seawater desalination system for cogeneration power plants. Desalination. 217 (2007) 191-202.
[16] M. Meratizaman, S. Monadizadeh, M. Amidpour. Introduction of an efficient small-scale freshwater-power generation cycle (SOFC–GT–MED), simulation, parametric study and economic assessment. Desalination. 351 (2014) 43-58.
[17] B. Najafi, A. Shirazi, M. Aminyavari, F. Rinaldi, R.A. Taylor. Exergetic, economic and environmental analyses and multi-objective optimization of an SOFC-gas turbine hybrid cycle coupled with an MSF desalination system. Desalination. 334 (2014) 46-59.
[18] H. Mokhtari, M. Sepahvand. Thermoeconomic and exergy analysis in using hybrid systems (GT+ MED+ RO) for desalination of brackish water in Persian Gulf. Desalination. 399 (2016) 1-15.
[19] M. Shamoushaki, M. Ehyaei, F. Ghanatir. Exergy, economic and environmental analysis and multi-objective optimization of a SOFC-GT power plant. Energy. 134 (2017) 515-31.
[20] S. Khanmohammadi, K. Atashkari. Modeling and multi-objective optimization of a novel biomass feed polygeneration system integrated with multi effect desalination unit. Thermal Science and Engineering Progress. 8 (2018) 269-83.
[21] M. Moghimi, M. Emadi, A.M. Akbarpoor, M. Mollaei. Energy and exergy investigation of a combined cooling, heating, power generation, and seawater desalination system. Applied Thermal Engineering. 140 (2018) 814-27.
[22] H. Rashidi, J. Khorshidi. Exergy analysis and multiobjective optimization of a biomass gasification based multigeneration system. International Journal of Hydrogen Energy. 43 (2018) 2631-44.
[23] H. Ghaebi, S. Ahmadi. Energy and exergy evaluation of an innovative hybrid system coupled with HRSG and HDH desalination units. Journal of Cleaner Production. 252 (2020) 119821.

[24] K. Mohammadi, M.S.E. Khaledi, M. Saghafifar, K. Powell. Hybrid systems based on gas turbine combined cycle for trigeneration of power, cooling, and freshwater: A comparative techno-economic assessment. Sustainable Energy Technologies and Assessments. 37 (2020) 100632.
[25] S. Georgousopoulos, K. Braimakis, D. Grimekis, S. Karellas. Thermodynamic and techno-economic assessment of pure and zeotropic fluid ORCs for waste heat recovery in a biomass IGCC plant. Applied Thermal Engineering. 183 (2021) 116202.
[26] M. Vojdani, I. Fakhari, P. Ahmadi. A novel triple pressure HRSG integrated with MED/SOFC/GT for cogeneration of electricity and freshwater: Techno-economic-environmental assessment, and multi-objective optimization. Energy Conversion and Management. 233 (2021) 113876.
[27] M. Zoghi, H. Habibi, A. Chitsaz, S.G. Holagh. Multi-criteria analysis of a novel biomass-driven multi-generation system including combined cycle power plant integrated with a modified Kalina-LNG subsystem employing thermoelectric generator and PEM electrolyzer. Thermal Science and Engineering Progress. 26 (2021) 101092.
[28] Y. Cao, H.A. Dhahad, H. Togun, A.E. Anqi, N. Farouk, B. Farhang. A novel hybrid biomass-solar driven triple combined power cycle integrated with hydrogen production: Multi-objective optimization based on power cost and CO2 emission. Energy Conversion and Management. 234 (2021) 113910.
[29] M.L. Kamari, A. Maleki, M.A. Nazari, M. Sadeghi, M.A. Rosen, F. Pourfayaz. Assessment of a biomass-based polygeneration plant for combined power, heat, bioethanol and biogas. Applied Thermal Engineering. 198 (2021) 117425.
[30] U. Safder, H.-T. Nguyen, P. Ifaei, C. Yoo. Energetic, economic, exergetic, and exergorisk (4E) analyses of a novel multi-generation energy system assisted with bagasse-biomass gasifier and multi-effect desalination unit. Energy. 219 (2021) 119638.
[31] M. Jalili, R. Ghasempour, M.H. Ahmadi, A. Chitsaz, S.G. Holagh. An integrated CCHP system based on biomass and natural gas co-firing: exergetic and thermo-economic assessments in the framework of energy nexus. Energy Nexus. (2021) 100016.
[32] Y. Cao, H.A. Dhahad, H. Togun, A.E. Anqi, N. Farouk, B. Farhang. Proposal and thermo-economic optimization of using LNG cold exergy for compressor inlet cooling in an integrated biomass fueled triple combined power cycle. International Journal of Hydrogen Energy. 46 (2021) 15351-66.
[33] Y.-P. Xu, Z.-H. Lin, T.-X. Ma, C. She, S.-M. Xing, L.-Y. Qi, et al. Optimization of a biomass-driven Rankine cycle integrated with multi-effect desalination, and solid oxide electrolyzer for power, hydrogen, and freshwater production. Desalination. 525 (2022) 115486.
[34] F. Musharavati, A. Khoshnevisan, S.M. Alirahmi, P. Ahmadi, S. Khanmohammadi. Multi-objective optimization of a biomass gasification to generate electricity and desalinated water using Grey Wolf Optimizer and artificial neural network. Chemosphere. 287 (2022) 131980.
[35] M. Ehyaei, A. Mozafari, M. Alibiglou. Exergy, economic & environmental (3E) analysis of inlet fogging for gas turbine power plant. Energy. 36 (2011) 6851-61.
[36] M. Ehyaei, S. Hakimzadeh, N. Enadi, P. Ahmadi. Exergy, economic and environment (3E) analysis of absorption chiller inlet air cooler used in gas turbine power plants. International Journal of Energy Research. 36 (2012) 486-98.
[37] M. Ehyaei, M.A. Rosen. Optimization of a triple cycle based on a solid oxide fuel cell and gas and steam cycles with a multiobjective genetic algorithm and energy, exergy and economic analyses. Energy conversion and management. 180 (2019) 689-708.
[38] K.H. Mistry, M.A. Antar, J.H. Lienhard V. An improved model for multiple effect distillation. Desalination and Water Treatment. 51 (2013) 807-21.
[39] M. Shamoushaki, D. Fiaschi, G. Manfrida, L. Talluri. Energy, exergy, economic and environmental (4E) analyses of a geothermal power plant with NCGs reinjection. Energy. (2021) 122678.
[40] A. Bejan. Advanced engineering thermodynamics. John Wiley & Sons, Hoboken, New Jersey, 2016.

[41] S. Jarungthammachote, A. Dutta. Thermodynamic equilibrium model and second law analysis of a downdraft waste gasifier. Energy. 32 (2007) 1660-9.
[42] S. Soltani, S.M.S. Mahmoudi, M. Yari, M.A. Rosen. Thermodynamic analyses of a biomass integrated fired combined cycle. Applied Thermal Engineering. 59 (2013) 60-8.
[43] P. Talebizadehsardari, M.A. Ehyaei, A. Ahmadi, D.H. Jamali, R. Shirmohammadi, A. Eyvazian, et al. Energy, exergy, economic, exergoeconomic, and exergoenvironmental (5E) analyses of a triple cycle with carbon capture. Journal of CO2 Utilization. 41 (2020) 101258.
[44] F.N. Alasfour, M.A. Darwish, A.O. Bin Amer. Thermal analysis of ME-TVC+MEE desalination systems. Desalination. 174 (2005) 39-61.
[45] I.S. Al-Mutaz, I. Wazeer. Development of a steady-state mathematical model for MEE-TVC desalination plants. Desalination. 351 (2014) 9-18.
[46] O. Miyatake, K. Murakami, Y. Kawata, T. Fujii. Fundamental experiments with flash evaporation. Heat Transfer-Jpn Res. 2 (1973) 89-100.
[47] H.T. El-Dessouky, H.M. Ettouney. Fundamentals of salt water desalination. Elsevier2002.
[48] F.N. Alasfour, M.A. Darwish, A.O. Bin Amer. Thermal analysis of ME—TVC+MEE desalination systems. Desalination. 174 (2005) 39-61.
[49] H. El-Dessouky, H. Ettouney, F. Al-Juwayhel. Multiple effect evaporation—vapour compression desalination processes. Chemical Engineering Research and Design. 78 (2000) 662-76.
[50] G.P. Thiel, A. Kumar, A. Gómez-González, J.H. Lienhard. Utilization of desalination brine for sodium hydroxide production: technologies, engineering principles, recovery limits, and future directions. ACS Sustainable Chemistry & Engineering. 5 (2017) 11147-62.
[51] A. Lazzaretto, G. Tsatsaronis. SPECO: a systematic and general methodology for calculating efficiencies and costs in thermal systems. Energy. 31 (2006) 1257-89.
[52] A. Bejan, G. Tsatsaronis, M. Moran. Thermal Design and Optimization John Wiley and Sons. Inc New York. (1996).
[53] T.J. Kotas. The exergy method of thermal plant analysis. Elsevier2013.
[54] E. Bellos, S. Pavlovic, V. Stefanovic, C. Tzivanidis, B.B. Nakomcic-Smaradgakis. Parametric analysis and yearly performance of a trigeneration system driven by solar-dish collectors. International Journal of Energy Research. 43 (2019) 1534-46.
[55] C. Tzivanidis, E. Bellos, K.A. Antonopoulos. Energetic and financial investigation of a stand-alone solar-thermal Organic Rankine Cycle power plant. Energy conversion and management. 126 (2016) 421-33.
[56] H. Nami, I.S. Ertesvåg, R. Agromayor, L. Riboldi, L.O. Nord. Gas turbine exhaust gas heat recovery by organic Rankine cycles (ORC) for offshore combined heat and power applications-Energy and exergy analysis. Energy. 165 (2018) 1060-71.
[57] H. Nami, E. Akrami. Analysis of a gas turbine based hybrid system by utilizing energy, exergy and exergoeconomic methodologies for steam, power and hydrogen production. Energy Conversion and Management. 143 (2017) 326-37.
[58] Water pricing for public supply. 2021.
[59] Sodium hydroxide. 2021.
[60] Hydrochloric Acid. 2021.
[61] Estimated landed prices of LNG worldwide as of March 2021, by select country 2021.
[62] A.H. Mosaffa, N. Hasani Mokarram, L. Garousi Farshi. Thermoeconomic analysis of a new combination of ammonia/water power generation cycle with GT-MHR cycle and LNG cryogenic exergy. Applied Thermal Engineering. 124 (2017) 1343-53.
[63] S. Khanmohammadi, K. Atashkari, R. Kouhikamali. Exergoeconomic multi-objective optimization of an externally fired gas turbine integrated with a biomass gasifier. Applied Thermal Engineering. 91 (2015) 848-59.

[64] M.H. Karimi, N. Chitgar, M.A. Emadi, P. Ahmadi, M.A. Rosen. Performance assessment and optimization of a biomass-based solid oxide fuel cell and micro gas turbine system integrated with an organic Rankine cycle. International Journal of Hydrogen Energy. 45 (2020) 6262-77.
[65] J.L. Silveira, C.E. Tuna. Thermoeconomic analysis method for optimization of combined heat and power systems. Part I. Progress in Energy and Combustion Science. 29 (2003) 479-85.
[66] M.L. Elsayed, O. Mesalhy, R.H. Mohammed, L.C. Chow. Exergy and thermo-economic analysis for MED-TVC desalination systems. Desalination. 447 (2018) 29-42.
[67] L. Pierobon, T.-V. Nguyen, U. Larsen, F. Haglind, B. Elmegaard. Multi-objective optimization of organic Rankine cycles for waste heat recovery: Application in an offshore platform. Energy. 58 (2013) 538-49.
[68] A. Bejan, G. Tsatsaronis, M.J. Moran. Thermal design and optimization. John Wiley & Sons1995.
[69] T. Shafer. Calculating Inflation Factors for Cost Estimates. City of Lincoln Transportation and Utilities Project Delivery.
[70] Statista. Global inflation rate compared to previous year.
[71] S. Edalati, M. Ameri, M. Iranmanesh, H. Tarmahi, M. Gholampour. Technical and economic assessments of grid-connected photovoltaic power plants: Iran case study. Energy. 114 (2016) 923-34.
[72] B. Kanagarajan. Emission and energy analysis of self-sufficient biomass power plant to achieve near net zero CO 2 emission. Mechanical engineering. Missouri university2015. p. 82.
[73] P. Basu. Biomass gasification and pyrolysis: practical design and theory. First ed. Academic press2010.
[74] A. Razmi, M. Soltani, M. Tayefeh, M. Torabi, M.B. Dusseault. Thermodynamic analysis of compressed air energy storage (CAES) hybridized with a multi-effect desalination (MED) system. Energy Conversion and Management. 199 (2019) 112047.
[75] A. Naseri, M. Bidi, M.H. Ahmadi, R. Saidur. Exergy analysis of a hydrogen and water production process by a solar-driven transcritical CO2 power cycle with Stirling engine. Journal of Cleaner Production. 158 (2017) 165-81.